



Review

Progress and Perspective of Glass-Ceramic Solid-State Electrolytes for Lithium Batteries

Liyang Lin ^{1,2,3,4,*} , Wei Guo ¹, Mengjun Li ¹, Juan Qing ⁴, Chuang Cai ^{1,2,3}, Ping Yi ^{1,2,3}, Qibo Deng ⁵  and Wei Chen ^{1,2,3}

¹ School of Aeronautics, Chongqing Jiaotong University, Chongqing 400074, China

² Chongqing Key Laboratory of Green Aviation Energy and Power, Chongqing 401130, China

³ The Green Aerotechnics Research Institute, Chongqing Jiaotong University, Chongqing 401120, China

⁴ School of Materials Science and Engineering, Chongqing Jiaotong University, Chongqing 400074, China

⁵ Key Laboratory of Hebei Province on Scale-Span Intelligent Equipment Technology, Tianjin Key Laboratory of Power Transmission and Safety Technology for New Energy Vehicles, School of Mechanical Engineering, Hebei University of Technology, Tianjin 300401, China

* Correspondence: jack_linliyang@cqjtu.edu.cn

Abstract: The all-solid-state lithium battery (ASSLIB) is one of the key points of future lithium battery technology development. Because solid-state electrolytes (SSEs) have higher safety performance than liquid electrolytes, and they can promote the application of Li-metal anodes to endow batteries with higher energy density. Glass-ceramic SSEs with excellent ionic conductivity and mechanical strength are one of the main focuses of SSE research. In this review paper, we discuss recent advances in the synthesis and characterization of glass-ceramic SSEs. Additionally, some discussions on the interface problems commonly found in glass-ceramic SSEs and their solutions are provided. At the end of this review, some drawbacks of glass-ceramic SSEs are summarized, and future development directions are prospected. We hope that this review paper can help the development of glass-ceramic solid-state electrolytes.

Keywords: lithium batteries; glass-ceramic; solid electrolyte; synthesis and characterization; high ionic conductivity



Citation: Lin, L.; Guo, W.; Li, M.; Qing, J.; Cai, C.; Yi, P.; Deng, Q.; Chen, W. Progress and Perspective of Glass-Ceramic Solid-State Electrolytes for Lithium Batteries. *Materials* **2023**, *16*, 2655. <https://doi.org/10.3390/ma16072655>

Academic Editor: Toshinori Okura

Received: 5 March 2023

Revised: 21 March 2023

Accepted: 26 March 2023

Published: 27 March 2023



Copyright: © 2023 by the authors. Licensee MDPI, Basel, Switzerland. This article is an open access article distributed under the terms and conditions of the Creative Commons Attribution (CC BY) license (<https://creativecommons.org/licenses/by/4.0/>).

1. Introduction

Since Sony first commercialized lithium-ion batteries (LIBs) in 1991, LIBs have been widely used in electronics, power and energy storage applications due to their high working voltage, high energy density, long cycle life and no memory characteristics [1–3]. With the rapid development of electric vehicles (EVs), traditional LIBs have been insufficient to meet the range of EVs. The energy density of traditional LIBs has achieved 260 Wh·kg^{−1}, which is approaching the limitations of traditional LIBs [4]. Metal lithium has a high theoretical specific capacity (3860 mAh·g^{−1}) and the lowest redox potential (−3.04 V vs. SHE) and can effectively increase the energy density of the battery when used as the anode [5]. However, traditional liquid electrolytes restrict the application of the lithium-metal anode because they contain flammable organic solvents that cause some safety problems [6,7]. All-solid-state lithium-metal batteries (ASSLMBs) with higher safety and higher energy density composed of lithium-metal anodes and solid-state electrolytes (SSEs) instead of traditional liquid electrolytes are expected to become the next generation of lithium battery.

In 1833, Faraday first discovered the ionic conductivity of solid Ag₂S and PbF₂, and research on the ionic conductivity of solids has been conducted since that time [8]. In the 1960s, Na₂O·11Al₂O₃ with Na⁺ ion conductivity was discovered, and researchers discovered that this type of material possessed the property of high ionic conductivity and had the potential to be used as SSEs [9]. Therefore, using solids with satisfactory ionic conductivity to form ASSLIBs became possible. SSEs, the most important component of ASSLIBs, have many advantages over liquid electrolytes.

- The non-flammable characteristics of SSEs make ASSLIBs have higher safety performance than LIBs [10].
- Compared to traditional LIBs, SSEs are able to replace the liquid electrolyte and separator to effectively reduce battery weight. Meanwhile, the energy density of the battery is increased by combining the application of a lithium-metal anode [11].
- Compared to conventional LIBs, ASSLIBs have greater structural design advantages because they can be connected in series internally to achieve higher voltages. Chen et al. [12] stacked one, two and three solid-state cells in a button battery to obtain open-circuit voltages of 3.08, 6.51 and 9.12 V, respectively.

Although ASSLIBs have certain advantages, their process of industrialization is still limited by technological, marketing and financial factors. On the technological side, the research of SSE synthesis method, stability, conductivity and interfacial properties is the key to practical application. After years of development, SSEs can be divided into three categories: inorganic solid electrolytes (ISEs), polymer solid electrolytes (PSEs) and composite solid electrolytes (CSEs). Among them, ISEs can be divided into amorphous glass, glass-ceramic and polycrystalline ceramic. Glass is an amorphous supercooled liquid, while glass-ceramics are partially crystalline glasses, consisting of a mixture of crystalline and amorphous glass phases [13,14]. The definition of glass-ceramic materials is an inorganic non-metal material prepared by controlling the crystallization of glass through different processing methods [15]. They consist of at least one functional crystalline phase and residual glass. The volume fraction of the crystalline part in glass-ceramic materials is typically in the range of 10–90% [14]. The main advantages of glass-ceramic materials are their dense, non-porous microstructure, and good mechanical, electrical and thermal properties. Glass-ceramic SSEs have become one of the hot research directions for SSEs due to their excellent ionic conductivity, electrochemical properties and better compatibility with electrodes.

Glass-ceramic SSEs are divided into two main categories, oxide glass-ceramic SSE systems and sulfide glass-ceramic SSE systems. Oxide glass-ceramic SSEs include NASICON-type electrolytes and some other oxides. They are mainly prepared by the melt-quenching method with subsequent heat treatment, and their main advantages are high ionic conductivity (10^{-4} – 10^{-3} S·cm⁻¹), large Li⁺ transference number and high mechanical strength [16,17]. The sulfide glass-ceramic SSEs are mainly Li₂S–P₂S₅ binary systems, which are prepared by mechanical ball milling and subsequent heat treatment, and their main advantages are high ionic conductivity (10^{-3} – 10^{-2} S·cm⁻¹) [18–21]. Although glass-ceramic SSEs generally have high ionic conductivity, the stability of the SSE itself and the interface problems between the electrode/electrolyte are major impediments to the practical application of ASSLIBs [22,23]. Improving the properties including ionic conductivity and chemical stability has become one of the main focuses of current research on glass-ceramic SSEs.

In this review, first, the synthesis and characterization of glass-ceramic electrolytes in recent years will be summarized. At the same time, the ionic conduction mechanism and the high ionic conductivity of glass-ceramic SSEs will be introduced briefly in this work. Then, we will discuss the common interface problem between SSEs and electrodes and summarize the performance of glass-ceramic SSEs and the corresponding solutions to the interface problem. We hope to provide reference for the development of the ASSLIB industry by reviewing the research progress of glass-ceramic SSEs and looking forward to their application prospects.

2. Ionic Conduction Mechanism

For designing high-performance SSEs, an understanding of their ion conduction mechanisms is necessary. Li⁺ ion migration in ceramics relies on different types of defects, including point defects, line defects, planar defects, volume defects and electron defects. Compared to other defects, point defects have a greater impact on cation transport in

crystals [24]. In a perfectly ordered crystal, ions cannot leave their host position [8]. The migration of ions in SSEs is accomplished by moving point defects in the crystal.

The basic assumption about the ionic conduction mechanism in polycrystalline (ceramic) is that vacancies in the lattice and interstitial spaces in the cationic sublattice are considered as charged movable species [25,26]. It is noteworthy that only a fraction of cations in a lattice has an ability to move having vacant stable or meta-stable lattice nodes within reach [9]. Currently, there are three main types of cation migration, as shown in Figure 1.

- Cation vacancy diffusion, cation migration from the initial position to its adjacent vacancy lattice position.
- The cation occupying the interstitial migrates directly to the adjacent vacant interstitial.
- Interstitialcy mechanism, cation occupying a lattice interstitial migrates to an adjacent lattice node, migrating the cation occupying that lattice to the next site.

For polycrystalline ceramic SSEs, the Li^+ transport mechanism depends on three factors: carrier type, diffusion pathways and diffusion type. The carrier type and concentration are determined by the point defects in the polycrystalline ceramic structure, which directly affect the ionic conductivity. The interactions between Li ions during migration in the crystal and between ones and the surrounding environment will significantly affect the ionic conductivity [24,27–29].

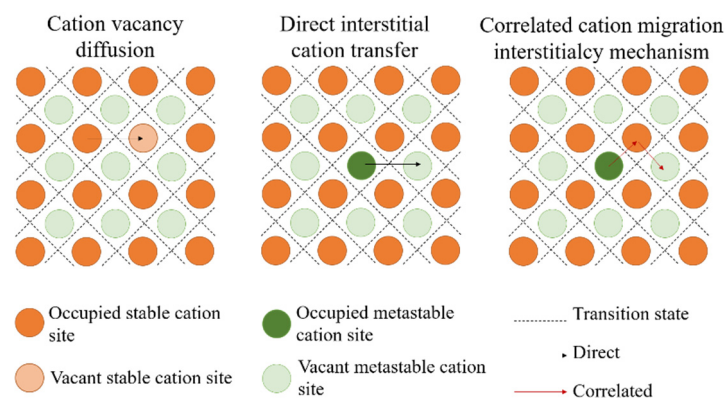


Figure 1. Three typical cation migration mechanisms: cation vacancy diffusion, direct interstitial cation transfer, correlated cation migration interstitialcy mechanism. Reprinted with permission from ref. [26]. Copyright 2019 Springer Nature.

Compared to ceramic SSEs, amorphous (glass) SSEs have better flexibility, uniformity and density. Meanwhile, the glass SSEs show no grain boundary resistance and isotropic Li^+ mobility. These properties of glass SSEs have prompted attempts to find its ionic conduction mechanism. At present, although many experimental data on Li^+ conduction in glass SSEs are available, the Li^+ conduction mechanism in glass SSEs is still not well explained, and no relevant general theory has been established. The main challenge is that glass SSEs are a short-range ordered, long-range disordered amorphous material. It means that the glass SSEs have no long-range crystalline order, no regular symmetric long-range ion migration pathways and no regular symmetric short-range coordination order [9]. In glass SSEs with disordered structure, the migration of cations in SSEs cannot be explained by a single factor. During the migration of cations in glass SSEs, charge carrier interactions and even interactions with the transport matrix can have an effect on the migration of ions. This makes the theoretical development of the conduction mechanism of cations in glass SSEs difficult. However, hypotheses have been offered to explain how the cations migrate in the amorphous SSE [30].

Funke et al. [31] suggested that structure and kinetic disorder are major factors in the high ionic conductivity of amorphous materials. They defined the movement of ions in a completely ordered crystal structure as level 1. This material is regarded as an insulator

without ion movement because of the absence of defects in the perfectly ordered crystal structure. Crystal structures with few defects are defined as level 2, and a single point defect can only move randomly to another location. Materials with disordered structure are defined as level 3, and ion movement cannot be described by defect theory but is related to multiple interactions with the surrounding environment. They suggested that the mismatch caused by the hopping of ions resulted in rearrangement of the particles of the neighborhood. The hopping ion is accommodated by the new site created by its neighborhood relaxation.

3. Synthesis and Characterization of Glass-Ceramic Solid-State Electrolytes

Currently, there are two main types of glass-ceramic SSEs, oxide glass-ceramic SSE systems and sulfide glass-ceramic SSE systems. Glass-ceramic SSEs are mainly prepared in two steps by the melt-quenching method and mechanical ball-milling method. In the first step, the required parent glass is prepared at a given ratio of raw materials by high temperature melting or mechanical ball milling. In the second step, the parent glass is heat-treated between the glass transition temperature T_g and the crystallization temperature T_c . T_g and T_c are determined by differential thermal analysis (DTA) and differential scanning calorimetry (DSC). Currently, glass-ceramic materials with high ionic conductivity are mainly obtained by changing the optimized raw material ratio, heat treatment temperature and time. Glass-ceramic SSEs prepared by wet chemical methods have also been reported recently [32–35]. For the prepared glass-ceramic SSEs, the properties were investigated mainly by characterization means such as impedance spectroscopy (IS), X-ray diffraction (XRD), DTA, DSC and electron microscopy. In some cases, short-range ordering in glass-ceramic SSEs has also been investigated by nuclear magnetic resonance (NMR). In this chapter, the preparation and characterization of oxide glass-ceramic SSE systems and sulfide glass-ceramic SSE systems are highlighted in the following sections. Additionally, possible ways to improve their ionic conductivity will be discussed.

3.1. Oxide Glass-Ceramic SSE Systems

Most of the oxide SSEs are polycrystalline ceramic SSEs whose advantages are high ionic conductivity, high mechanical strength and a wide electrochemical stability window. However, the interface problem between this type of SSEs and electrodes is more prominent. Compared to polycrystalline ceramics, glass has certain advantages in terms of flexibility, homogeneity and density. Therefore, glass-ceramic SSEs are prepared by fusion glass and partial crystallization of glass, which not only improve the ionic conductivity but also optimize the interface between SSEs and electrodes to some extent. The current research on oxide glass-ceramic SSE systems is mainly focused on Na^+ superionic conductor (NASICON)-type SSEs and some other types of oxides.

3.1.1. NASICON-Type Glass-Ceramic Systems

In 1976, the NASICON-type compound was first discovered by Goodenough et al. [36]. The chemical formula is $\text{NaM}_2(\text{PO}_4)_3$ (M is a tetravalent metal [M^{4+}], e.g., Ge, Ti, Sn and Zr [37]). $\text{Na}_{1+x}\text{Zr}_2\text{Si}_x\text{P}_{3-x}\text{O}_{12}$ ($0 < x < 3$) which is called NASICON and is obtained when the P is partially replaced by Si. Their structures have a rhombic crystal lattice, space group R-3c, but for some compounds the trigonal distortion of the lattice was found [22,38]. Figure 2 shows a typical crystal structure of this type of compound, which consists of stacked (or joint) MO_6 octahedra and PO_4 tetrahedra [39]. The charge carriers in the structure can occupy two different six-coordinated positions, M1 between two MO_6 octahedra and M2 in the eight-coordination position between two rows of MO_6 octahedra. Li^+ migrates in the ion channel formed by M1 and M2 under the influence of the electric field, and all positions of the occupied part form the 3D channel of Li^+ [40,41]. Li^+ conduction can be achieved by replacing Na with Li while maintaining the crystal structure, and the most representative one is $\text{LiTi}_2(\text{PO}_4)_3$ [42]. Lithium analogues of NASICON-type compounds are heavily investigated as promising SSEs for ASSLIBs.

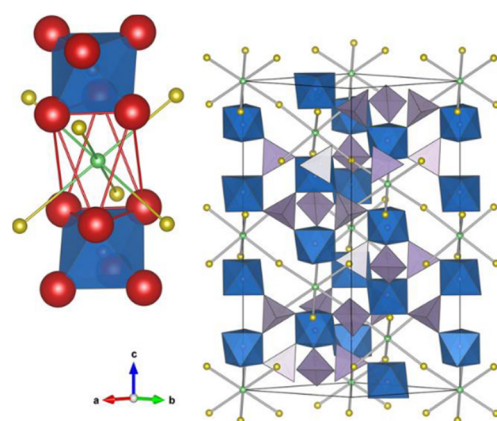


Figure 2. Representations of a typical NASICON structure. Blue octahedra are MO_6 units, purple tetrahedra are PO_4 units, green spheres are M1 sites and yellow spheres are M2 sites. Reprinted with permission from ref. [41]. Copyright 2014 American Chemical Society.

In recent years, there are mainly two types of NASICON-type SSEs, LATP and LAGP. The representative materials for LATP and LAGP are $\text{Li}_{1.3}\text{Al}_{0.3}\text{Ti}_{1.7}(\text{PO}_4)_3$ [43] and $\text{Li}_{1.5}\text{Al}_{0.5}\text{Ge}_{1.5}(\text{PO}_4)_3$ [44], respectively. The ionic conductivity of SSEs is mainly affected by the preparation process, microstructure and porosity. Due to the open framework structure of NASICON, this type of SSE generally suffers from high porosity and high grain boundary resistance, which leads to the low total conductivity of SSEs [16,45]. The low void fraction of glass-ceramic materials can improve their cation migration properties. At the same time, glass-ceramic materials have better conductive interface regions on newly formed crystalline grains embedded in the glass matrix, and the grain boundary resistance can be effectively reduced by controlling the crystallization of the parent glass. Therefore, the electrical properties of NASICON-type glass-ceramic SSEs can be well improved as a result of optimizing the synthesis conditions.

In most studies, scholars have mainly used the melt-quenching method [46–49] to prepare NASICON-type glass-ceramic SSEs, which is divided into three main steps: (1) the mixture of raw materials is melted at high temperatures to form precursors, (2) rapid cooling to form the parent glass and (3) after annealing to release stress, the glass undergoes a period of heat treatment to nucleate and grow NASICON crystals. The control and optimization of various parameters are very important for the preparation of glass-ceramic SSEs by the melt-quenching method, such as the composition ratio of elements, and the temperature of crystallization and annealing [50]. An improper elemental composition ratio can lead to the formation of impurity phases in NASICON glass-ceramic SSEs, which can hinder the migration of Li^+ ions leading to a decrease in ionic conductivity. In contrast, a proper crystallization temperature can result in glass-ceramic SSEs with low void fraction and grain boundary resistance. Illbeigi et al. [51] synthesized $\text{Li}_{1+x+y}\text{Al}_x\text{Cr}_y\text{Ge}_{2-x-y}(\text{PO}_4)_3$ by melt quenching ($x + y = 0.5$, $y = 0, 0.1, 0.25, 0.4, 0.5$ and $x = 0.5, 0.4, 0.25, 0.1, 0$) glass-ceramic SSEs. It was found that the addition of Cr can increase the crystal cell dimension, thus increasing their electrical conductivity. The prepared $\text{Li}_{1.5}\text{Al}_{0.4}\text{Cr}_{0.1}\text{Ge}_{1.5}(\text{PO}_4)_3$ glass-ceramics not only have a high ionic conductivity but also show an excellent electrochemical stability window up to 7 V vs. Li/Li^+ . However, when the content of Cr > 0.1, the authors found the impure phases GeO_2 and CrPO_4 in the grain boundaries by XRD and FESEM. Additionally, the impure phase hinders the migration of Li^+ ions and causes a decrease in the ionic conductivity of the materials; the XRD patterns are shown in Figure 3a. The maximum Li^+ conductivity of $\text{Li}_{1.5}\text{Al}_{0.4}\text{Cr}_{0.1}\text{Ge}_{1.5}(\text{PO}_4)_3$ sample was $6.65 \times 10^{-3} \text{ S}\cdot\text{cm}^{-1}$ at 26 °C, as shown in Figure 3b. Zhu et al. [52] prepared $\text{Li}_{1.5}\text{Al}_{0.5}\text{Ge}_{1.5}(\text{PO}_4)_3$ glass-ceramic SSEs by the melt-quenching method, and the effects of different crystallization temperatures were investigated by XRD, SEM and NMR. SEM images are shown in Figure 3c. The results show that the formation of amorphous phases, cracks and voids can be effectively controlled by adjusting the crystallization temperature, thus improving the ion transport at the grain

boundaries. Nikodimos et al. [53] prepared Sc-doped $\text{Li}_{1+x+y}\text{Al}_x\text{Sc}_y\text{Ge}_{2-x-y}(\text{PO}_4)_3$ by melt quenching and found that it has high ionic conductivity and good contact properties with the anode. Meanwhile, the material also showed an electrochemical stability window of up to 7.5 V vs. Li/Li^+ .

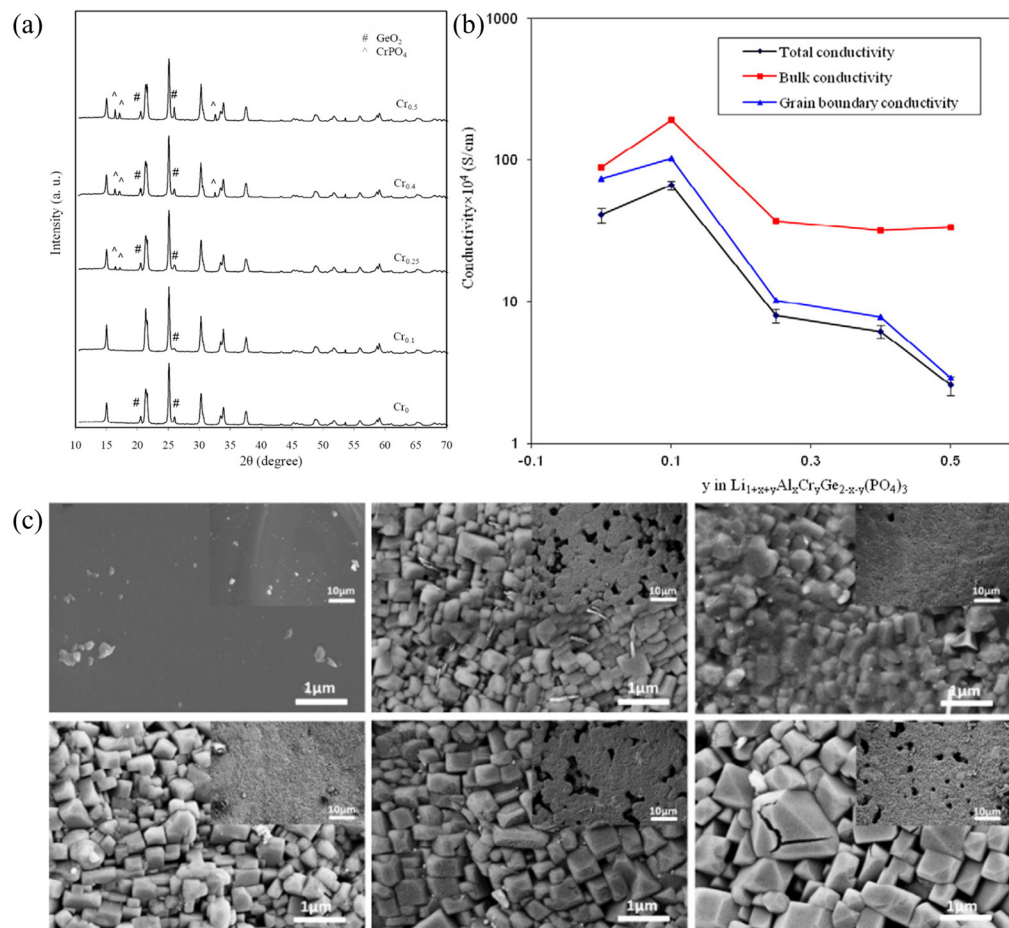


Figure 3. (a) XRD patterns of samples with different Cr contents crystallized at 850 °C for 8 h; (b) The total, bulk and grain boundary conductivities measured at 26 °C for $\text{Li}_{1+x+y}\text{Al}_x\text{Cr}_y\text{Ge}_{2-x-y}(\text{PO}_4)_3$ samples with different Cr contents. Reprinted with permission from ref. [51]. Copyright 2016 Elsevier. (c) SEM micrographs of LAGP samples in glass phase and crystallized at 750 °C, 775 °C, 800 °C, 825 °C, 850 °C. Reprinted with permission from ref. [52]. Copyright 2015 Elsevier.

The melt-quenching method for the preparation of NASICON-type glass-ceramic SSEs is still the mainstream preparation method today, and some recent studies on the preparation of NASICON-type glass-ceramic SSEs by melt quenching are summarized in Table 1. However, other methods have also been used to prepare this type of glass-ceramic SSE. Yi et al. [54] prepared $\text{Li}_{1.7}\text{Al}_{0.3}\text{Ti}_{1.7}\text{Si}_{0.4}\text{P}_{2.6}\text{O}_{12}$ glass-ceramic SSEs by the liquid-feed flame spray pyrolysis (LF-FSP) process, and the ionic conductivity reached $7.7 \times 10^{-4} \text{ S}\cdot\text{cm}^{-1}$ at room temperature. In addition, microwave sintering [55], spark plasma sintering [56] and hot-press sintering [57] methods for the preparation of NASICON-type glass-ceramic SSEs have been reported.

Table 1. Review of various parameters of NASICON-type glass-ceramic materials prepared by melt-quenching method in recent years.

| Composition | T _g (°C) | T _c (°C) | Crystallization | σ (S·cm ^{−1}) | E _a (eV) | Reference |
|--|---------------------|---------------------|-----------------|--------------------------------|---------------------|-----------|
| Li _{1.3} Al _{0.3} Ti _{1.7} (PO ₄) ₃ | 624 | 660 | 1000 °C/0.33 h | 1.3×10^{-3} | 0.27 | [43] |
| Li _{1.3} Al _{0.3} Ti _{1.7} (PO ₄) ₃ | 640 | 670 | 950 °C/70 h | 1.23×10^{-4} | 0.37 | [58] |
| Li _{1.3} Al _{0.3} Ti _{1.7} (PO ₄) ₃ ·50P ₂ O ₅ | 632 | 750 | 850 °C/10 h | 8.5×10^{-4} | 0.26 | [59] |
| Li _{1.4} Al _{0.4} Ge _{1.6} (PO ₄) ₃ | 534 | 614 | 650 °C/96 h | 3.8×10^{-5} | 0.52 | [60] |
| Li _{1.5} Al _{0.5} Ge _{1.5} (PO ₄) ₃ | 508.4 | 598.4 | 820 °C/2 h | 5.03×10^{-4} | 0.36 | [44] |
| Li _{1.5} Al _{0.5} Ge _{1.5} (PO ₄) ₃ | 524 | 589 | 800 °C/8 h | 2.9×10^{-3} | 0.29 | [52] |
| Li _{1.25} Al _{0.25} Sn _{0.25} Ge _{1.75} (PO ₄) ₃ | 518 | 622 | 628 °C/1 h | 3.9×10^{-5} | 0.36 | [61] |
| Li _{1.5} Al _{0.33} Sc _{0.17} Ge _{1.5} (PO ₄) ₃ | | | 800 °C/8 h | 5.8×10^{-3} | 0.28 | [53] |
| Li _{1.5} Al _{0.5} Ge _{1.5} (PO ₄) ₃ + 0.05Li ₂ O | 532 | 629 | 829 °C/6 h | 7.3×10^{-4} | 0.38 | [62] |
| Li _{1.5} Al _{0.5} Ge _{1.5} (PO ₄) ₃ ·0.05B ₂ O ₃ | 526.0 | 636.4 | 820 °C/2 h | 5.5×10^{-4} | | [63] |
| Li _{1.4} Cr _{0.4} Ge _{0.64} Ti _{0.96} (PO ₄) ₃ | 623 | 692 | 900 °C/12 h | 6.6×10^{-5} | 0.40 | [64] |
| Li _{1.6} Cr _{0.6} Ge _{0.28} Ti _{1.12} (PO ₄) ₃ | 682.5 | 725.8 | 900 °C/2 h | 2.9×10^{-4} | 0.26 | [65] |

3.1.2. Other Oxide Glass-Ceramic Systems

In addition to NASICON compounds, there are other oxides that can be used as SSEs. These oxide glass-ceramic SSEs are prepared by different methods, such as mechanochemical methods and melt-quenching methods. Mechanochemical preparation of glass-ceramic SSEs is mechanically treating the raw material to convert mechanical energy to the energy of chemical reaction [66–68]. Tatsumisago et al. [69] obtained 90Li₃BO₃·10Li₂SO₄ glass-ceramic SSEs with an ionic conductivity of 1.4×10^{-5} S·cm^{−1} by the mechanochemical method at room temperature, as shown in Figure 4a. Yoneda et al. [70] prepared 90Li₄SiO₄·10Li₂SO₄ glass-ceramic SSEs by the mechanochemical method, and then assembled ASSLIBs with Li-In/LiNi_{1/3}Mn_{1/3}Co_{1/3}O₂ without high-temperature sintering. The melt-quenching method also can be used to prepare oxide glass-ceramic SSEs. Widanarto et al. [71] prepared (85 − x)TeO₂·xLi₂O·15ZnO (x = 0, 5, 10, 15 mol%) by the melt-quenching method; SEM images are shown in Figure 4b. The study indicates that high-quality zinc-tellurite glass-ceramic SSEs with improved ionic conductivity can be obtained by proper control of temperature, AC frequency (AC) and Li₂O concentration. Tezuka et al. [72] prepared Li₄B₇O₁₂Cl glass-ceramic SSEs by the melt-quenching method with an ionic conductivity of 4.6×10^{-4} S·cm^{−1} at 200 °C and the conductivity activation energy was 0.52 eV.

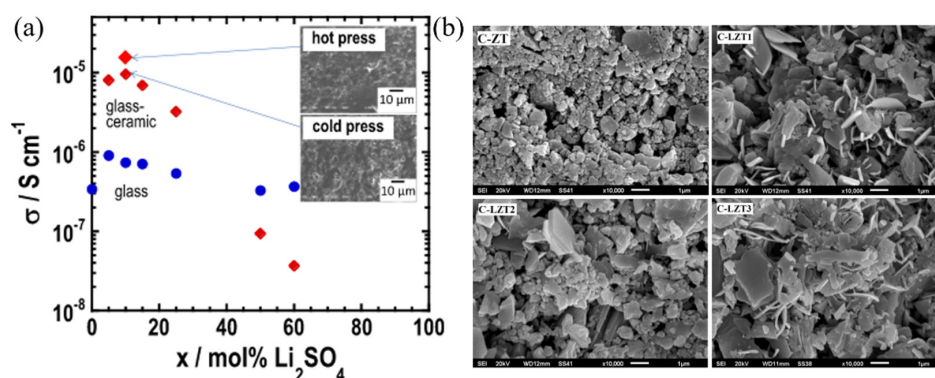


Figure 4. (a) Composition dependence of the ionic conductivity at room temperature of mechanochemically prepared Li₃BO₃·Li₂SO₄ glasses and the corresponding glass precursors heat-treated at temperatures just above the first crystallization peak. The inset shows SEM photographs of compressed particles of Li_{2.9}B_{0.9}S_{0.1}O_{3.1} powder prepared by cold pressing at room temperature and hot pressing at 255 °C. Reprinted with permission from ref. [69]. Copyright 2014 Elsevier. (b) SEM images of the prepared (85 − x)TeO₂·xLi₂O·15ZnO (x = 0, 5, 10, 15 mol%) glass-ceramic electrolytes. Reprinted with permission from ref. [71]. Copyright 2017 Elsevier.

In addition to the two preparation methods already presented, oxide glass-ceramic SSEs can also be prepared by other methods. Nagao et al. [73] prepared $90\text{Li}_3\text{BO}_3 \cdot 7\text{Li}_2\text{SO}_4 \cdot 3\text{Li}_2\text{CO}_3$ glass-ceramic SSEs by the mechanical ball-milling method with an ionic conductivity of $1 \times 10^{-5} \text{ S} \cdot \text{cm}^{-1}$ at room temperature. Okumura et al. [74] prepared $\text{Li}_{2.2}\text{C}_{0.8}\text{B}_{0.2}\text{O}_3$ glass-ceramic SSEs by the spark plasma sintering (SPS) process. The Li^+ conductivity at 30°C was $2.1 \times 10^{-6} \text{ S} \cdot \text{cm}^{-1}$. Shin et al. [75] prepared garnet-type $\text{Li}_7\text{La}_3\text{Zr}_2\text{O}_{12}$ -8wt% Li_3BO_3 glass-ceramic SSEs by low-temperature sintering using Li_3BO_3 glass-ceramic as a sintering additive with an ionic conductivity of $1.94 \times 10^{-5} \text{ S} \cdot \text{cm}^{-1}$ at room temperature.

3.2. Sulfide Glass-Ceramic SSE Systems

Compared to oxide SSEs, sulfide SSEs have been intensively studied in recent years due to their advantages such as higher ionic conductivity at room temperature and cheaper raw material. Sulfides can be processed into three forms: glass, glass-ceramic and crystalline. Glass-ceramic SSEs generally have better performance than the other two forms. Therefore, the sulfide glass-ceramic SSE system, represented by the glass-ceramic SSEs in the Li_2S - P_2S_5 binary system (LPS glass-ceramic SSEs), has been studied extensively in recent years.

3.2.1. Li_2S - P_2S_5 Binary System

The Li_2S - P_2S_5 binary system has several compounds, including $\text{Li}_2\text{P}_2\text{S}_6$, $\text{Li}_4\text{P}_2\text{S}_6$, $\text{Li}_7\text{P}_3\text{S}_{11}$ and Li_3PS_4 , as shown in Figure 5 [18]. In the $x\text{Li}_2\text{S}$ -($100 - x$) P_2S_5 (x , molar percent) system, $x\text{Li}_2\text{S}$ -($100 - x$) P_2S_5 glass-ceramic SSEs containing $70\% < x < 80\%$ were the most studied, for example, $70\text{Li}_2\text{S}$ - $30\text{P}_2\text{S}_5$ [76], $75\text{Li}_2\text{S}$ - $25\text{P}_2\text{S}_5$ [77] and $78\text{Li}_2\text{S}$ - $22\text{P}_2\text{S}_5$ [78]. Therefore, we only briefly introduce the crystal structures of $\text{Li}_7\text{P}_3\text{S}_{11}$ and Li_3PS_4 .

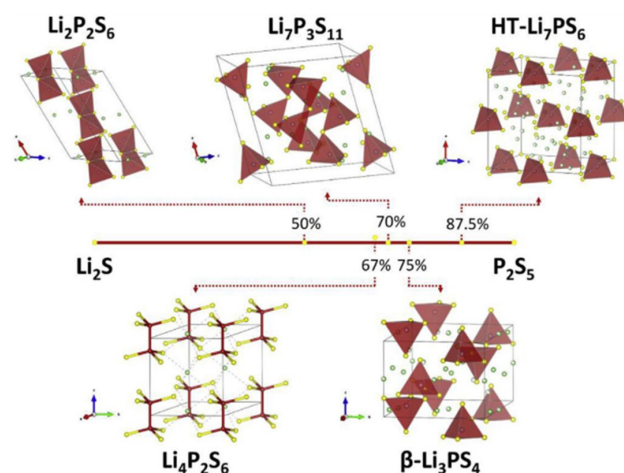


Figure 5. Some of the crystal structures observed in materials, formed within Li_2S - P_2S_5 binary system. Reprinted with permission from ref. [18]. Copyright 2018 Elsevier.

$\text{Li}_7\text{P}_3\text{S}_{11}$ is usually obtained from $70\text{Li}_2\text{S}$ - $30\text{P}_2\text{S}_5$ by heat treatment and has a very high Li^+ conductivity with low room temperature conduction activation energy [76]. Its crystal structure has trigonal symmetry, space group P-1, with two $\text{Li}_7\text{P}_3\text{S}_{11}$ units per cell [18]. The crystal structure can be regarded as consisting of PS_4^{3-} tetrahedra and $\text{P}_2\text{S}_7^{4-}$ 4-bis-tetrahedra, and Li^+ is mainly distributed in the interstices between the tetrahedra and bis-tetrahedra [79]. Ceder et al. [80] considered that the tetrahedra composed of S^{2-} in $\text{Li}_7\text{P}_3\text{S}_{11}$ are face-centered cubic-stacked, which can provide a lower conduction activation energy and facilitate the rapid transport of Li^+ .

Li_3PS_4 belongs to the Li_2S - P_2S_5 binary system of $75\text{Li}_2\text{S}$ - $25\text{P}_2\text{S}_5$, which is assembled into ASSLIBs under the same conditions and has better cycling performance than $\text{Li}_7\text{P}_3\text{S}_{11}$ [81]. Li_3PS_4 has four main crystalline forms: β - Li_3PS_4 , γ - Li_3PS_4 , α - Li_3PS_4 and δ - Li_3PS_4 . In 2011, Homma et al. [82] reported β - Li_3PS_4 by heating the γ - Li_3PS_4 to 300°C . Although β - Li_3PS_4 did not receive much attention initially, β - Li_3PS_4 glass-ceramic SSEs

synthesized by ball milling were later found to have high ionic conductivity. It is now commonly believed that β - Li_3PS_4 consists of hexagonally close-packed sulfide ions with Li and P in the generated interstitials. It is suggested that the distortion of the close-packed arrangement due to the difference in size and binding properties of Li and P is responsible for the higher ionic conductivity of β - Li_3PS_4 than γ - Li_3PS_4 [80].

3.2.2. Synthesis of LPS Glass-Ceramic SSEs

Currently, most of the reported LPS glass-ceramic SSEs have been prepared mainly by mechanical ball milling. Mechanical ball treatment can be controlled by the proportion of the reagents and milling beads, milling speed and time in order to carry out the chemical process [83]. The material prepared by this process is usually in the glassy state and requires heat treatment of the parent glass to crystallize it in order to obtain the glass-ceramic SSEs. Kim et al. [84] prepared $78.3\text{Li}_2\text{S}\cdot 21.7\text{P}_2\text{S}_5$ with an ionic conductivity of $6.3 \times 10^{-4} \text{ S}\cdot\text{cm}^{-1}$ at room temperature by the mechanical ball-milling method and subsequent heat treatment. During heat treatment, it is extremely important to control the temperature and time of the heat treatment to control the crystal microstructure and, thus, improve the performance of the electrolyte. Lu et al. [85] successfully controlled the microstructure of $75\text{Li}_2\text{S}\cdot 25\text{P}_2\text{S}_5$ based on the precipitation kinetics and effective medium approach and prepared the sample by mechanical ball milling. The microstructure of the prepared SSEs was well controlled, and its electrical conductivity increased by 80%. The LPS glass-ceramic SSEs prepared by this method were also used to assemble ASSLIBs with good cell performance. Yu et al. [86] prepared $\text{Li}_7\text{P}_3\text{S}_{11}$ by the mechanical ball-milling method and subsequent annealing heat treatment for assembling ASSLIBs with $\text{Li}_2\text{S}/\text{Li}_7\text{P}_3\text{S}_{11}/\text{Li-In}$ structure. The ASSLIBs provided a discharge specific capacity of $1139.5 \text{ mAh g}^{-1}$ during the initial cycle and still maintained a discharge specific capacity of 850.0 mAh g^{-1} after 30 cycles. Wang et al. [87] also prepared $\text{Li}_7\text{P}_3\text{S}_{11}$ by the mechanical ball-milling method as well as heat treatment and assembled Li-S cells with $\text{FeS}_2/\text{Li}_7\text{P}_3\text{S}_{11}/\text{Li-In}$ structure, which provided 620.8 mAh g^{-1} initial discharge capacity at 0.1C at room temperature.

It may be supposed that the heat generated by the high-energy collision between the raw material and the grinding medium at room temperature is sufficient to partially melt and recrystallize the material. Trevey et al. [88] successfully prepared $\text{Li}_2\text{S-GeS}_2\text{-P}_2\text{S}_5$ glass-ceramic SSEs by the SSBM process for the assembly of ASSLIBs with a $\text{Li}/\text{Li}_2\text{S-GeS}_2\text{-P}_2\text{S}_5/\text{LiCoO}_2$ structure, which exhibited a discharge capacity at the second cycle of 129 mAh g^{-1} . In addition to the mechanical ball-milling method, the melt-quenching method can also be used to prepare LPS glass-ceramic SSEs. Seino et al. [89] prepared the parent glass by melt quenching. The glass powder was compressed at 94 MPa first, and then heated at 280°C or 300°C for 2 h. The prepared $70\text{Li}_2\text{S}\cdot 30\text{P}_2\text{S}_5$ glass-ceramic sample had a very high ionic conductivity of $1.7 \times 10^{-2} \text{ S}\cdot\text{cm}^{-1}$ at room temperature and a minimum conduction activation energy of $17 \text{ kJ}\cdot\text{mol}^{-1}$, as shown in Figure 6a. Preefer et al. [90] prepared $\text{Li}_7\text{P}_3\text{S}_{11}$ samples by using a rapid assisted-microwave procedure, which showed good ionic conductivity at room temperature.

In addition, the liquid-phase synthesis method allows the preparation of more homogeneous electrolyte materials and also has the potential for large-scale industrial preparation [32]. Therefore, the preparation of LPS glass-ceramic SSEs by liquid-phase synthesis is a new method in recent years. The method is based on the addition of raw materials to organic solvents, followed by heat treatment to remove the organic solvents, and finally sintering the products to produce LPS glass-ceramic SSEs. Xu et al. [33] first ground the raw materials into powder, then dispersed the powder in acetonitrile (ACN) solution separately, and prepared $\text{Li}_7\text{P}_3\text{S}_{11}$ samples by two-step heat treatment. The preparation process is shown in Figure 6b. At room temperature, this sample showed an ionic conductivity of $9.7 \times 10^{-4} \text{ S}\cdot\text{cm}^{-1}$ and a low activation energy of $31.2 \text{ kJ}\cdot\text{mol}^{-1}$. Calpa et al. [34] prepared the $\text{Li}_7\text{P}_3\text{S}_{11}$ sample by liquid-phase treatment under ultrasonic treatment, achieving a high ionic conductivity of $1.0 \times 10^{-3} \text{ S}\cdot\text{cm}^{-1}$ at 22°C and a low activation energy of $31.2 \text{ kJ}\cdot\text{mol}^{-1}$. Choi et al. [35] prepared $75\text{Li}_2\text{S}\cdot 25\text{P}_2\text{S}_5$ glass-ceramic SSEs using the low-

temperature solution technique (LTST), which reduced the ionic conductivity of this type of material but increased the interface area between the LiCoO_2 cathode and $75\text{Li}_2\text{S}-25\text{P}_2\text{S}_5$ electrolyte, thus improving the cycling performance of the battery.

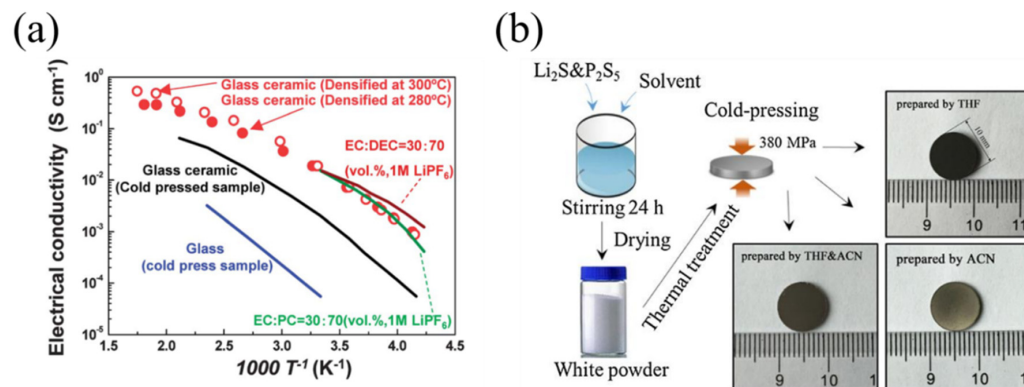


Figure 6. (a) Plots of ionic conductivity versus temperature for $70\text{Li}_2\text{S}-30\text{P}_2\text{S}_5$, cold-pressed glass, glass-ceramic powder and some common liquid electrolytes prepared by melt-quenching method. Reprinted with permission from ref. [89]. Copyright 2014 Royal Society of Chemistry. (b) Preparation process of $\text{Li}_7\text{P}_3\text{S}_{11}$ samples by liquid phase synthesis. Reprinted with permission from ref. [33]. Copyright 2016 Elsevier.

3.2.3. Enhancement of LPS Glass-Ceramic Performance

LPS glass-ceramic SSEs have high ionic conductivity, but most still fall short of existing organic liquid electrolytes. Meanwhile, LPS glass-ceramic SSEs are more sensitive to moisture. Once in a humid environment, they can produce toxic H_2S gas leading to structural changes in the electrolyte as well as the decay of ionic conductivity [91]. In addition, LPS glass-ceramic SSEs also generally suffer from a narrow electrochemical window. Therefore, it is necessary to adopt some methods to enhance the various performance of LPS glass-ceramic SSEs to promote their practical application.

Currently, most of the research reports focus on the enhancement of various properties of LPS glass-ceramic SSEs by doping methods. This method is mainly used to enhance the performance of the electrolyte by creating defects in the crystal structure of the material and expanding the Li^+ transport channels. In the reported studies, the main doped substances include oxides, sulfides, halogenated compounds and some other compounds [92,93]. In addition to single-phase doping, two-phase co-doping or even three-phase doping can be used to improve the performance of LPS. In conclusion, optimization of each property including ionic conductivity, material stability and interfacial properties with electrodes is the key to optimizing material properties by doping. Oxides including Li_2ZrO_3 [94], LiSO_4 [95], Li_2O [96], ZnO [97], LiNO_3 [98] and Nb_2O_5 [99] can effectively enhance the ionic conductivity performance of SSEs materials by doping. $70\text{Li}_2\text{S}-(30-x)\text{P}_2\text{S}_5-x\text{Li}_3\text{PO}_4$ was successfully prepared by Huang et al. [100], exhibiting $1.87 \times 10^{-3} \text{ S cm}^{-1}$ with a minimum activation energy of 18 kJ/mol when $x = 1\%$ mol. The assembled $\text{Li-In}/70\text{Li}_2\text{S}-29\text{P}_2\text{S}_5-1\text{Li}_3\text{PO}_4/\text{LiCoO}_2$ cell exhibited a discharge specific capacity of 108 mAh g^{-1} , as shown in Figure 7a. The impedance spectrum EIS analysis revealed that the doping with Li_3PO_4 reduced the interfacial resistance between the electrode and electrolyte, as shown in Figure 7b. Lu et al. [94] prepared $99(70\text{Li}_2\text{S}-30\text{P}_2\text{S}_5)-1\text{Li}_2\text{ZrO}_3$ glass-ceramic SSEs with a high ionic conductivity of $2.85 \times 10^{-3} \text{ S cm}^{-1}$. After being assembled into ASSLIBs, they exhibited a higher cell cycling performance. Tsukasaki et al. [101] successfully prepared $(100-x)\text{Li}_3\text{PS}_4-x\text{ZnO}$, and found that Li_3PS_4 doped with 10% or 20% ZnO could better balance the performance of thermal stability, moisture resistance and ionic conductivity by DSC analysis.

In addition to oxides, sulfides including GeS_2 [102], P_2S_3 [103], SnS_2 [104], Ni_3S_2 [105] and LiSnS_4 [106] can also be used for the doping of LPS glass-ceramic SSEs. $(100-x)(70\text{Li}_2\text{S}-$

$30\text{P}_2\text{S}_5$)- $x\text{FeS}_2$ glass-ceramic SSEs were prepared by Zhou et al. [107] and then characterized by solid-state NMR. It was found that FeS_2 doping could controllably adjust the crystalline part in the glass-ceramic SSEs to achieve excellent ionic conductivity, as shown in Figure 7c. Cells with the structure FeS_2 composite/ $99.5(70\text{Li}_2\text{S}-30\text{P}_2\text{S}_5)$ - 0.5FeS_2 /Li–Ln showed higher initial capacity and better cycling performance than those with the structure FeS_2 composite/ $70\text{Li}_2\text{S}-30\text{P}_2\text{S}_5$ /Li–Ln. Otoyama et al. [108] added LiSnS_4 into Li_3PS_4 to form the LiSnS_4 - Li_3PS_4 system, which improved the ionic conductivity as well as the air stability of the glass-ceramic SSEs without affecting the electrochemical stability. Halogen compounds such as LiX ($\text{X} = \text{F}, \text{Cl}, \text{Br}, \text{I}$) [109,110] and $\text{Li}(\text{BH}_4)_{0.75}\text{I}_{0.25}$ [111], etc., are also widely used for doping. Tatsumisago et al. [112] systematically investigated the doping effect of LiX ($\text{X} = \text{F}, \text{Cl}, \text{Br}, \text{I}$) on $\text{Li}_7\text{P}_3\text{S}_{11}$, and their results showed that the doping with LiBr was most effective in enhancing the ionic conductivity of $\text{Li}_7\text{P}_3\text{S}_{11}$ glass-ceramic SSEs. Further study by Zhao et al. [113] showed that LiBr does not enter the lattice but exists in the interstices between the $\text{Li}_7\text{P}_3\text{S}_{11}$ lattice. The high electronegativity of Br reduces the electron cloud density on the surface of $\text{P}_2\text{S}_7^{4-}$ and PS_4^{3-} units, decreasing their binding to Li^+ , and, thus, increasing the ionic conductivity.

With the in-depth study of doping methods, multiphase co-doped LPS glass-ceramic SSEs have also been reported in recent years. Zhang et al. [114] investigated $\text{Li}_7\text{P}_3\text{S}_{11}$ glass-ceramic SSEs co-doped with WS_2 and LiBr by dielectric spectroscopy, and their results showed that the doped LPS-based glass-ceramic SSEs had synergistic effects in terms of ionic conductivity and interfacial compatibility. Wang et al. [115] successfully prepared Zn-, Br- and I-substituted $\text{LPSZn}_{0.05}\text{Br}_{0.2}\text{I}_{0.8}$ glass-ceramic SSEs with high ionic conductivity as well as low activation energy at room temperature, as shown in Figure 7d. Additionally, the Li^+ conductivity can be enhanced by adding a certain amount of Li as a charge carrier to the $\text{Li}_{7+x}\text{P}_3\text{S}_{11}$ glass-ceramic SSEs [116]. The ionic conductivity can also be improved by reducing the grain boundaries of the material through hot-press densification and adjusting and optimizing the heat treatment parameters in the material preparation method [89,117].

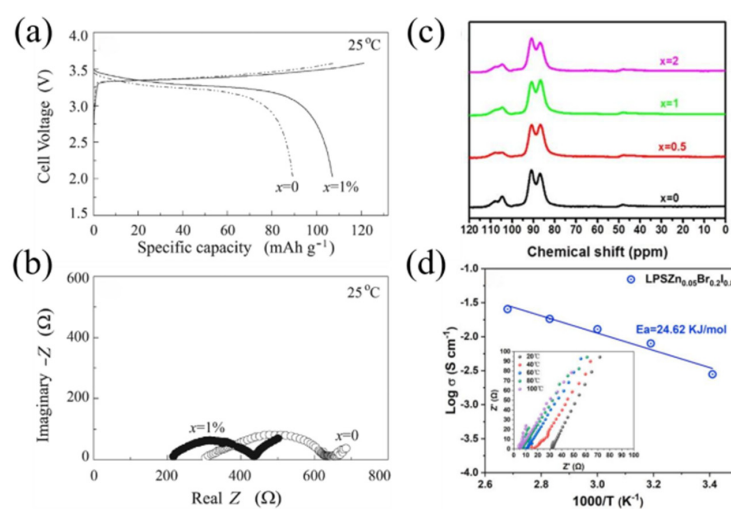


Figure 7. (a) Charge and discharge curves of $\text{Li-In}/70\text{Li}_2\text{S}-(30-x)\text{P}_2\text{S}_5-x\text{Li}_3\text{PO}_4/\text{LiCoO}_2$ battery; (b) electrochemical impedance spectra of $\text{Li-In}/70\text{Li}_2\text{S}-(30-x)\text{P}_2\text{S}_5-x\text{Li}_3\text{PO}_4/\text{LiCoO}_2$ battery. Reprinted with permission from ref. [100]. Copyright 2019 Elsevier. (c) The ^{31}P MAS NMR spectra of $(100-x)(70\text{Li}_2\text{S}-30\text{P}_2\text{S}_5)$ - $x\text{FeS}_2$ ($x = 0, 0.5, 1, 2$) glass-ceramic samples. Reprinted with permission from ref. [107]. Copyright 2020 Elsevier. (d) Conductivity and impedance data for $\text{LPSZn}_{0.05}\text{Br}_{0.2}\text{I}_{0.8}$ glass-ceramic SSEs. Reprinted with permission from ref. [115]. Copyright 2022 Elsevier.

The recent studies on LPS electrolytes are summarized, including ionic conductivity, energy density of assembled cells and electrochemical window, as shown in Table 2. The data presented in Table 2 show that doping, optimization of preparation methods and some other methods can significantly improve the properties of LPS glass-ceramic SSEs.

Table 2. Review of the various properties of LPS glass-ceramic SSE in recent years.

| Composition | σ (S·cm ⁻¹) | Structure of the Battery | Initial Energy Density | Electrochemical Window | Ref |
|---|--------------------------------|---|---|----------------------------------|-------|
| 70Li ₂ S·30P ₂ S ₅ | 1.7×10^{-2} | | | −0.1~5 V vs. Li/Li ⁺ | [89] |
| Li ₇ P ₃ S ₁₁ | 6.3×10^{-4} | Li ₂ S/Li ₇ P ₃ S ₁₁ /Li-In | 1139.5 mAh/g at 0.064 mA/cm ² | | [86] |
| Li ₇ P ₃ S ₁₁ | 1.27×10^{-3} | FeS ₂ /Li ₇ P ₃ S ₁₁ /Li-In | 620.8 mAh/g at 0.1C | | [87] |
| Li ₇ P ₃ S ₁₁ | 9.7×10^{-4} | | | −0.5~5 V vs. Li/Li ⁺ | [33] |
| Li ₇ P ₃ S ₁₁ | 1.0×10^{-3} | | | −0.5~5 V vs. Li/Li ⁺ | [34] |
| Li _{7.25} P ₃ S ₁₁ | 2.5×10^{-3} | LiNi _{0.8} Co _{0.15} Al _{0.05} O ₂ / Li _{7.25} P ₃ S ₁₁ /In | 106.2 mAh/g at 0.1C | 2.0~3.6 V vs. Li-In | [116] |
| 99(70Li ₂ S·30P ₂ S ₅)-1Li ₂ ZrO ₃ | 2.85×10^{-3} | LiCoO ₂ /99(70Li ₂ S·30P ₂ S ₅)- 1Li ₂ ZrO ₃ /Li-In | 134.5 mAh/g at 0.1C | | [94] |
| Li ₇ P _{2.88} Nb _{0.12} S _{10.7} O _{0.3} | 3.59×10^{-3} | Li ₂ S/Li ₇ P _{2.88} Nb _{0.12} S _{10.7} O _{0.3} /Li | 642.1 mAh/g at 0.1C | | [99] |
| 70Li ₂ S·29P ₂ S ₅ -1Li ₃ PO ₄ | 1.87×10^{-3} | LiCoO ₂ / 70Li ₂ S·29P ₂ S ₅ -1Li ₃ PO ₄ /Li-In | 108 mAh/g at 0.1C | | [100] |
| 99.5(70Li ₂ S·30P ₂ S ₅)-0.5FeS ₂ | 2.22×10^{-3} | FeS ₂ composite/ 99.5(70Li ₂ S·30P ₂ S ₅)-0.5FeS ₂ /Li-Ln | 543 mAh/g at 0.03 mA/cm ² | −0.5~5 V vs. Li/Li ⁺ | [107] |
| 80Li ₇ P ₃ S ₁₁ -20LiBr | 3.39×10^{-3} | LiCoO ₂ /80Li ₇ P ₃ S ₁₁ -20LiBr/Li | 120 mAh/g at 0.1 mA/cm ² | | [113] |
| 90(0.7Li ₂ S-0.29P ₂ S ₅ - 0.01WS ₂)-10LiBr | | LiCoO ₂ /90(0.7Li ₂ S-0.29P ₂ S ₅ -0.01WS ₂)- 10LiBr/Li-In | 129.6 mAh/g at 0.1C | | [114] |
| 75Li ₂ S·25P ₂ S ₅ | 3.1×10^{-4} | LiCoO ₂ /75Li ₂ S·25P ₂ S ₅ /electrical conductive carbon | 115 mAh/g at 0.05C | −1~5 V vs. Li/Li ⁺ | [35] |
| Li _{3.06} P _{0.98} Zn _{0.02} S _{3.98} O _{0.02} | 1.12×10^{-3} | LiCoO ₂ /LGPS/Li _{3.06} P _{0.98} Zn _{0.02} S _{3.98} O _{0.02} /Li | 139.1 mAh/g at 0.1C | −0.5~6 V vs. Li/Li ⁺ | [97] |
| Li _{2.96} P _{0.98} S _{3.92} O _{0.06} -Li ₃ N | 1.58×10^{-3} | LiNbO ₃ @NCA/ Li _{2.96} P _{0.98} S _{3.92} O _{0.06} -Li ₃ N/Li | 107.89 mAh/g at 0.064 mA/cm ² | −0.5~5 V vs. Li/Li ⁺ | [98] |
| (Li ₂ S) ₉ -(P ₂ S ₅) ₃ -(Ni ₃ S ₂) ₁ (LPN 9:3:1) | 2.0×10^{-3} | LPN(9:3:1)-NCM/ LPN(9:3:1)/In | 117 mAh/g at 0.1C | −0.5~10 V vs. Li/Li ⁺ | [105] |
| 2.5Li ₃ PS ₄ -0.5Li ₄ SnS ₄ | 2.1×10^{-3} | LiCoO ₂ /2.5Li ₃ PS ₄ -0.5Li ₄ SnS ₄ /Li | 93 mAh/g at 0.1C | −0.1~5 V vs. Li/Li ⁺ | [106] |
| Li(BH ₄) _{0.75} I _{0.25} - (Li ₂ S) _{0.75} ·(P ₂ S ₅) _{0.25} | 1×10^{-3} | TiS ₂ /Li(BH ₄) _{0.75} I _{0.25} - (Li ₂ S) _{0.75} ·(P ₂ S ₅) _{0.25} /Li | 239 mAh/g at 0.05C | −0.5~5 V vs. Li/Li ⁺ | [111] |
| 78.3Li ₂ S·21.7P ₂ S ₅ | 6.3×10^{-4} | | | −0.3~5 V vs. Li/Li ⁺ | [84] |
| Li _{7.05} Zn _{0.05} P _{1.95} S ₈ Br _{0.2} I _{0.8} | 3.98×10^{-3} | | | −0.5~5 V vs. Li/Li ⁺ | [115] |

4. Interfacial Problems of Solid-State Electrolytes

Glass-ceramic SSEs have better interfacial properties than polycrystalline ceramic SSEs due to the presence of amorphous glass [20]. However, the interfacial problem between glass-ceramic SSEs and positive/negative electrodes is still an important challenge limiting the practical application of ASSLIBs [118]. Therefore, many studies on the interfacial properties of glass-ceramic SSEs with electrodes have also been reported. In this chapter, we will first briefly introduce the interfacial problem and its optimization methods, and then we will give an overview of the research on the interfacial properties of glass-ceramic SSEs.

4.1. Interface Problems and Optimization Methods

The interface problems between SSEs and electrodes include poor interfacial wettability and compatibility. This is manifested by a small interfacial contact area leading to insufficient contact, interfacial reactions and high interfacial resistance [119–123]. For ISEs, especially oxides, the interfacial problems are mainly due to high interfacial resistance caused by their rigid nature, poor electrode–electrolyte interfacial compatibility and technological difficulties [124]. For sulfide glass-ceramic SSEs, the poor stability in air is also responsible for their poor interfacial properties. This is due to the fact that sulfide glass-ceramic SSEs react with water in air to produce toxic H_2S gas, leading to the destruction of their structure, which leads to a series of problems such as the reduction in ionic conductivity [91]. In addition, consistency of composition and structure between the grain boundaries and the bulk phase are important for guaranteeing a low Li^+ transport resistance across the grain boundaries interface. Chemical composition and structural deviations would result in weak interactions between the framework and charge carriers, discontinuous pathways and a higher energy barrier for Li^+ conduction. [125]. The tight contact at the interface between the electrode and the SSEs is the key factor to improve the electrochemical performance of all ASSLIBs. There are three main aspects of current studies, including electrodes, electrolytes and the transition layer introduced between electrodes and SSEs to improve the interfacial properties.

For electrodes, designing an excellent composite electrode is important to enhance the interfacial properties [126]. Wang et al. [127] designed a Li-metal negative electrode with PEO-50000 (LiTFSI) film and obtained good interface by assembling into a cell of Li-PEO-500000 (LiTFSI)/LAGP-PEO1/LiMFP, as shown in Figure 8. Zhou et al. [128] then used organic quinone cathode 5,7,12,14-pentaerythritone (PT) to prepare an ASSLIB with a glass-ceramic $70\text{Li}_2\text{S}-30\text{P}_2\text{S}_5$ sulfide electrolyte, which exhibited excellent rate performance and cycling performance. The reason for this is that the inherently low Young's modulus of the PT electrode effectively prevents contact loss at the interface.

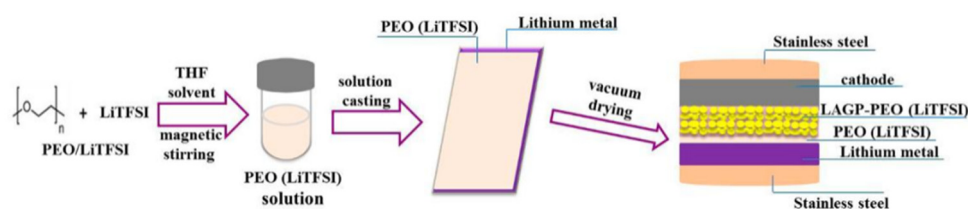


Figure 8. All-solid-state Li-PEO (LiTFSI)/LAGP-PEO (LiTFSI)/LiMFP cells. Reprinted with permission from ref. [127]. Copyright 2017 American Chemical Society.

The transition layer between the electrode and the SSEs can also enhance the interfacial properties [129,130]. Kato et al. [131] found that the insertion of Au films between the Li metal and the solid electrolyte can effectively maintain stable Li dissolution and deposition, thereby improving the utilization of Li-metal electrodes in all-solid-state batteries. Liang et al. [132] then introduced a Li^+ conduction buffer layer on the cathode surface to construct a well-matched interface between the cathode and SSEs.

In addition to the two mentioned methods, the interfacial properties between electrodes and SSEs can be enhanced by synthetic methods, modification of electrolytes and so on.

4.2. Enhancement of Interfacial Properties of Oxide Glass-Ceramic SSE Systems

The improvement of the interfacial properties of LATP and LAGP can be achieved in various ways, such as optimization of the preparation method, compounding with PSEs to form CSEs, introduction of thin films on the electrolyte surface and structural modifications. Structural modification of NASICON-type glass-ceramic SSEs is currently the most prominent method to enhance interfacial properties. Jadhav et al. [133] prepared LAGP glass-ceramic materials doped with B_2O_3 , and the B_2O_3 can stabilize LAGP in weak acid and weak base environments. Saffirio et al. [134] prepared $Li_{1.4}Al_{0.4}Ge_{0.4}Ti_{1.4}(PO_4)_3$ doped with 0.05% B_2O_3 and showed that the doping with B_2O_3 enhanced the anodic oxidation stability of the material and reduced the grain boundary resistance. This shows that the doping with B_2O_3 is helpful for the interfacial properties of LAGP-type glass-ceramic SSEs. Yamamoto et al. [135] successfully prepared LASGTP by co-doping LATP with Si and Ge, and cells with the structure of $LiCoO_2$ /LASGTP/Pt were assembled. The crystalline phases in the LASGTP glass matrix are composed of $Li_{1+x}Al_xGe_yTi_{2-x-y}P_3O_{12}$ (main-phase), $Li_{1+x+3z}Al_x(Ge,Ti)_{2-x}(Si_zPO_4)_3$ (sub-phase) and $AlPO_4$. They suggested that the insertion of Li into the LASGTP to form an amorphous phase and the gradual distribution of Li around the interface would lead to irreversible in situ formation of the anode in the LASGTP and produce low interfacial resistance.

The interfacial properties of NASICON-type glass-ceramic SSEs can also be improved by introducing thin films on the electrolyte surface. Liu et al. [136] sputtered amorphous Ge films on the LAGP surface, which not only inhibited the reduction reaction between Ge^{4+} and the Li-metal negative electrode, but also made a close contact between the Li-metal negative electrode and LAGP electrolyte. It was demonstrated by XPS characterization that the Ge film was formed only on the surface of SSEs, as shown in Figure 9a. Hu et al. [137] sputtered a metal Bi film on LAGP, which not only suppressed the unfavorable reaction between the LAGP electrolyte and Li-metal anode, but also improved their compatibility. The SEM image of the electrode–electrolyte interface cross-section is shown in Figure 9b.

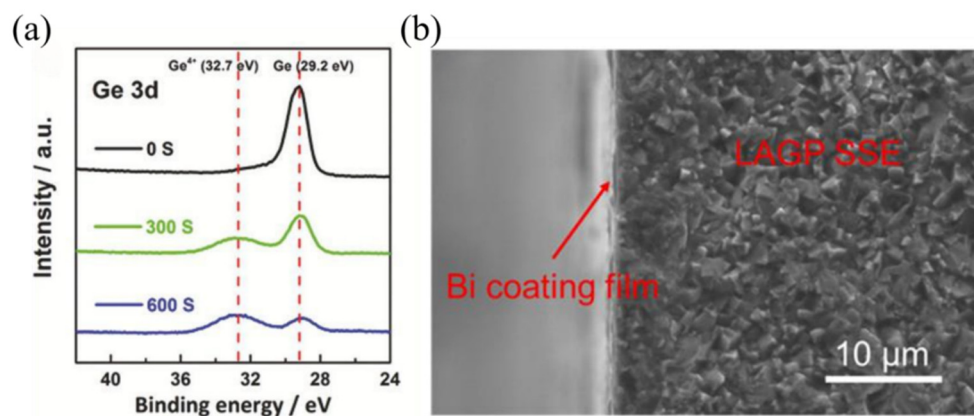


Figure 9. (a) XPS of the Ge film on LAGP pellet. Reprinted with permission from ref. [136]. Copyright 2018 WILEY-VCH Verlag GmbH & Co. KGaA, Weinheim. (b) Cross-sectional SEM image of the LAGP pellet coated with Bi buffer. Reprinted with permission from ref. [137]. Copyright 2020 American Chemical Society.

In addition, by improving the preparation methods such as heat treatment conditions, the interface properties can be improved to a certain extent [138]. The formation of CSE through the composite of glass-ceramic SSEs and PSEs is also a mainstream direction to improve the interfacial properties [139].

4.3. Enhancement of Interfacial Properties of Sulfide Glass-Ceramic SSE Systems

For sulfide glass-ceramic SSEs, the enhancement of the interfacial properties relies mainly on the structural modification by the dopants such as Fe_2S [107], $LiBr$ [113], $LiNO_3$ [98], LiI [109] and SeS_2 [140]. In the previous section, we focused on the performance

improvement of LPS glass-ceramic SSEs, so here we only present its improvement in interfacial properties. Feng et al. [141] successfully prepared new glass-ceramic SSEs of $\text{Li}_{10}\text{P}_3\text{S}_{12}\text{I}$ by mixing Li_2S , P_2S_5 and LiI in a certain ratio through solid-phase reaction. $\text{Li}_{10}\text{P}_3\text{S}_{12}\text{I}$ has higher interfacial stability and lower interfacial resistance than thiophosphate. This is mainly because $\text{Li}_{10}\text{P}_3\text{S}_{12}\text{I}$ generates LiI at the interface of the electrode as well as the electrolyte during the electrochemical cycle, and LiI contributes to the improvement of the interfacial stability. Additionally, it has been shown that the introduction of LiI could inhibit the growth of Li dendrites in LPS glass-ceramics, thus improving the cycling performance of the cell [109]. Wu et al. [140] successfully prepared SeS_2 -doped $70\text{Li}_2\text{S}$ - $30\text{P}_2\text{S}_5$, and observed the interface by EIS analysis and SEM. The result indicates that the addition of SeS_2 contributes to the reduction of the interfacial resistance, as shown in Figure 10a–d. Through the doping of LiNO_3 , Ahmad et al. [98] obtained a thermodynamically stable Li_2O and Li_3N solid electrolyte interface (SEI) at the interface between the electrode and the Li -metal anode, thus inhibiting the occurrence of interfacial reactions and the growth of Li dendrites.

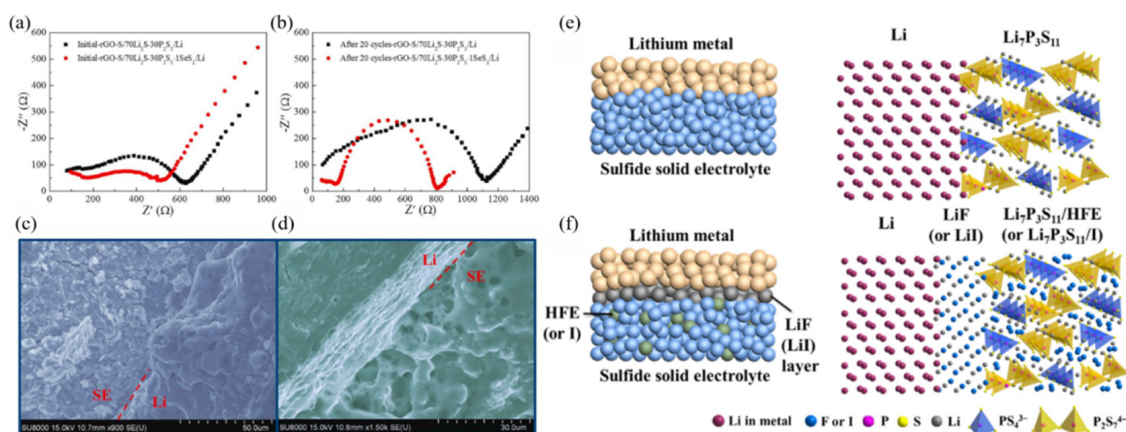


Figure 10. Nyquist plots of $\text{rGO}/70\text{Li}_2\text{S}-30\text{P}_2\text{S}_5/\text{Li}$ and $\text{rGO-S}/70\text{Li}_2\text{S}-29\text{P}_2\text{S}_5-1\text{SeS}_2/\text{Li}$ ASSLIBs at 30°C . Measurements were conducted (a) before and (b) after 20 cycles at $0.1 \text{ mA}\cdot\text{cm}^{-2}$; SEM images of the interface between the (c) $70\text{Li}_2\text{S}-30\text{P}_2\text{S}_5$, (d) $70\text{Li}_2\text{S}-29\text{P}_2\text{S}_5-1\text{SeS}_2$ and Li in $\text{rGO-S}/\text{solid electrolyte}/\text{Li}$ batteries at $0.1 \text{ mA}\cdot\text{cm}^{-2}$ for 100 charge–discharge cycles. Reprinted with permission from ref. [140]. Copyright 2019 Elsevier. Schematic diagrams of (e) $\text{Li}/\text{Li}_7\text{P}_3\text{S}_{11}$ interface of ASSLIBs and (f) modified interface with a uniform thin LiF (or LiI) interphase layer and HFE (or I solution) infiltrated sulfide electrolyte. Reprinted with permission from ref. [142]. Copyright 2018 Elsevier.

In addition to structural modifications, less research has been conducted to enhance the interfacial properties of LPS glass-ceramic SSEs by interfacial engineering of the coated films and optimization of the heat treatment conditions. Wei et al. [117] showed that the total interfacial resistance of $\text{Li}/\text{SE}/\text{Li}$ cells decreased by more than an order of magnitude with increasing heat treatment annealing temperature. However, too-high annealing temperature resulted in the formation of a low conductivity phase of $\text{Li}_4\text{P}_2\text{S}_6$ resulting in higher interfacial resistance. Xu et al. [142] assembled the $\text{LiNbO}_3@\text{LiCoO}_2/\text{Li}_7\text{P}_3\text{S}_{11}/\text{Li}$ cell using methoxyperfluorobutane (HFE)-coated/permeable $\text{Li}_7\text{P}_3\text{S}_{11}$ glass-ceramic SSEs with a LiF -coated Li -metal anode, showing high reversible discharge capacity as well as cycling performance, as shown in Figure 10e,f.

5. Conclusions and Perspective

Lithium batteries are widely used in power and energy storage applications due to their high energy density, good cycling performance and no memory characteristics. However, the current liquid electrolyte-based LIBs in the market are approaching the upper limit of their theoretical specific capacity and the safety issues will make it difficult to meet the future power needs of electric vehicles. The ASSLIBs based on SSEs can advance the

application of the Li-metal anode to make a Li battery with higher theoretical specific capacity and better safety performance. Glass-ceramic SSEs have both polycrystalline ceramic and amorphous glass phases, and, thus, have the advantages of high ionic conductivity, Li^+ transfer number and good interfacial properties. This review summarizes the recent research reports on glass-ceramic SSEs and briefly introduces the ion transfer mechanism, preparation methods, performance enhancement and their interfacial issues with electrodes. However, the current research reveals that glass-ceramic SSEs are still challenging from the perspective of practical application.

- Although the glass-ceramic SSE has a high ionic conductivity ($10^{-4}\sim 10^{-2} \text{ S}\cdot\text{cm}^{-1}$), there is still a gap to its practical application. This is mainly because LPS electrolyte materials still have problems such as water sensitivity and a narrow electrochemical window. Optimization of preparation methods and structural modifications are important to improve the properties of glass-ceramic SSEs.
- In addition to the properties of the materials themselves, the industrial production of the materials is another factor that hinders their practical application. Traditional solid-state reactions, mechanical ball milling and melt quenching require much time and effort. All these ways are difficult to apply to the practical production of glass-ceramic SSEs. The liquid-phase synthesis method seems to be a potential method for industrial production. However, for the present studies, the liquid-phase synthesis method is also not ready for practical production. Therefore, more research on industrial production methods for glass-ceramic SSEs is still necessary in the future.
- The small interfacial contact area caused by interfacial problems leads to poor contact, insufficient interfacial reactions and high interfacial resistance, which is still the most difficult obstacle to break through to further the practical application of ASSLIBs. The design of a good electrode/electrolyte contact interface through structural modification, interface engineering and optimization of preparation methods is the main way to improve the interfacial properties.

Overall, this review summarizes recent research on glass-ceramic SSEs in terms of preparation methods, characterization means, performance enhancement and electrode/electrolyte interface properties, hoping to assist in the research and practical application of ASSLIBs. Improving the performance of glass-ceramic SSE materials, expanding their production scale and designing excellent battery internal structures to promote safer and higher energy density batteries for practical applications are still the focus of future research.

Author Contributions: Conceptualization, L.L. and W.G.; methodology, M.L.; software, J.Q.; validation, C.C.; formal analysis, P.Y.; investigation, W.G.; writing—original draft preparation, W.G.; writing—review and editing, L.L. and Q.D.; visualization, W.G. and Q.D.; supervision, L.L. and W.C. All authors have read and agreed to the published version of the manuscript.

Funding: This work was financially supported by Science and Technology Research Program of Chongqing Municipal Education Commission (Grant No. KJZD-K202200702), and Natural Science Foundation of Chongqing (Grant No. cstc2021jcyj-msxmX0928).

Institutional Review Board Statement: Not applicable.

Informed Consent Statement: Not applicable.

Data Availability Statement: Not applicable.

Conflicts of Interest: The authors declare no conflict of interest.

References

1. La Monaca, A.; Paoletta, A.; Guerfi, A.; Rosei, F.; Zaghib, K. Electrospun ceramic nanofibers as 1D solid electrolytes for lithium batteries. *Electrochem. Commun.* **2019**, *104*, 106483. [[CrossRef](#)]
2. Manthiram, A. A reflection on lithium-ion battery cathode chemistry. *Nat. Commun.* **2020**, *11*, 1550. [[CrossRef](#)]

3. Yu, X.; Manthiram, A. A review of composite polymer-ceramtowardic electrolytes for lithium batteries. *Energy Storage Mater.* **2021**, *34*, 282–300. [[CrossRef](#)]
4. Li, W.D.; Song, B.H.; Manthiram, A. High-voltage positive electrode materials for lithium-ion batteries. *Chem. Soc. Rev.* **2017**, *46*, 3006–3059. [[CrossRef](#)]
5. Li, L.; Deng, Y.; Chen, G. Status and prospect of garnet/polymer solid composite electrolytes for all-solid-state lithium batteries. *J. Energy Chem.* **2020**, *50*, 154–177. [[CrossRef](#)]
6. Feng, J.; Wang, L.; Chen, Y.; Wang, P.; Zhang, H.; He, X. PEO based polymer-ceramic hybrid solid electrolytes: A review. *Nano Converg.* **2021**, *8*, 2. [[CrossRef](#)]
7. Li, S.; Zhang, S.; Shen, L.; Liu, Q.; Ma, J.; Lv, W.; He, Y.; Yang, Q. Progress and Perspective of Ceramic/Polymer Composite Solid Electrolytes for Lithium Batteries. *Adv. Sci.* **2020**, *7*, 1903088. [[CrossRef](#)] [[PubMed](#)]
8. Funke, K. Solid State Ionics: From Michael Faraday to green energy-the European dimension. *Sci. Technol. Adv. Mater.* **2013**, *14*, 043502. [[CrossRef](#)]
9. Kundu, S.; Kraysberg, A.; Ein-Eli, Y. Recent development in the field of ceramics solid-state electrolytes: I-oxide ceramic solid-state electrolytes. *J. Solid State Electrochem.* **2022**, *26*, 1809–1838. [[CrossRef](#)]
10. Zheng, Y.; Yao, Y.; Ou, J.; Li, M.; Luo, D.; Dou, H.; Li, Z.; Amine, K.; Yu, A.; Chen, Z. A review of composite solid-state electrolytes for lithium batteries: Fundamentals, key materials and advanced structures. *Chem. Soc. Rev.* **2020**, *49*, 8790–8839. [[CrossRef](#)] [[PubMed](#)]
11. He, F.; Tang, W.; Zhang, X.; Deng, L.; Luo, J. High energy density solid state lithium metal batteries enabled by sub-5 μm solid polymer electrolytes. *Adv. Mater.* **2021**, *33*, 2105329. [[CrossRef](#)] [[PubMed](#)]
12. Chen, X.; He, W.; Ding, L.X.; Wang, S.; Wang, H. Enhancing interfacial contact in all solid state batteries with a cathode-supported solid electrolyte membrane framework. *Energy Environ. Sci.* **2019**, *12*, 938–944. [[CrossRef](#)]
13. Sakamoto, A.; Yamamoto, S. Glass-Ceramics: Engineering Principles and Applications. *Int. J. Appl. Glass Sci.* **2010**, *1*, 237–247. [[CrossRef](#)]
14. Gandi, S.; Vaddadi, V.S.C.S.; Panda, S.S.S.; Goona, N.K.; Parne, S.R.; Lakavat, M.; Bhaumik, A. Recent progress in the development of glass and glass-ceramic cathode/ solid electrolyte materials for next-generation high capacity all-solid-state sodium-ion batteries: A review. *J. Power Sources* **2022**, *521*, 230930. [[CrossRef](#)]
15. Pietrzak, T.K.; Wasiucionek, M.; Garbarczyk, J.E. Towards Higher Electric Conductivity and Wider Phase Stability Range via Nanostructured Glass-Ceramics Processing. *Nanomaterials* **2021**, *11*, 1321. [[CrossRef](#)]
16. Dias, J.A.; Santagneli, S.H.; Messaddeq, Y. Methods for Lithium Ion NASICON Preparation: From Solid-State Synthesis to Highly Conductive Glass-Ceramics. *J. Phys. Chem. C* **2020**, *124*, 26518–26539. [[CrossRef](#)]
17. Jian, Z.; Hu, Y.; Ji, X.; Chen, W. NASICON-Structured Materials for Energy Storage. *Adv. Mater.* **2017**, *29*, 1601925. [[CrossRef](#)]
18. Kudu, Ö.U.; Famprikis, T.; Fleutot, B.; Braidia, M.-D.; Le Mercier, T.; Islam, M.S.; Masquelier, C. A review of structural properties and synthesis methods of solid electrolyte materials in the Li_2S – P_2S_5 binary system. *J. Power Sources* **2018**, *407*, 31–43. [[CrossRef](#)]
19. Lau, J.; DeBlock, R.H.; Butts, D.M.; Ashby, D.S.; Choi, C.S.; Dunn, B.S. Sulfide Solid Electrolytes for Lithium Battery Applications. *Adv. Energy Mater.* **2018**, *8*, 1800933. [[CrossRef](#)]
20. Hayashi, A.; Tatsumisago, M. Invited Paper: Recent Development of Bulk-Type Solid-State Rechargeable Lithium Batteries with Sulfide Glass-ceramic Electrolytes. *Electron. Mater. Lett.* **2012**, *8*, 199–207. [[CrossRef](#)]
21. Liu, D.; Zhu, W.; Feng, Z.; Guerfi, A.; Vijn, A.; Zaghbi, K. Recent progress in sulfide-based solid electrolytes for Li-ion batteries. *Mater. Sci. Eng. B* **2016**, *213*, 169–176. [[CrossRef](#)]
22. Hou, M.; Liang, F.; Chen, K.; Dai, Y.; Xue, D. Challenges and perspectives of NASICON-type solid electrolytes for all solid-state lithium batteries. *Nanotechnology* **2020**, *31*, 132003. [[CrossRef](#)] [[PubMed](#)]
23. Zhang, Q.; Cao, D.; Ma, Y.; Natan, A.; Aurora, P.; Zhu, H. Sulfide-Based Solid-State Electrolytes: Synthesis, Stability, and Potential for All-Solid-State Batteries. *Adv. Mater.* **2019**, *31*, 1901131. [[CrossRef](#)]
24. Yang, H.; Wu, N. Ionic conductivity and ion transport mechanisms of solid-state lithium-ion battery electrolytes: A review. *Energy Sci. Eng.* **2022**, *10*, 1643–1671. [[CrossRef](#)]
25. He, X.; Zhu, Y.; Mo, Y. Origin of fast ion diffusion in superionic conductors. *Nat. Commun.* **2017**, *8*, 15893. [[CrossRef](#)]
26. Famprikis, T.; Canepa, P.; Dawson, J.A.; Islam, M.S.; Masquelier, C. Fundamentals of inorganic solid-state electrolytes for batteries. *Nat. Mater.* **2019**, *18*, 1278–1291. [[CrossRef](#)]
27. Zhang, B.; Tan, R.; Yang, L.; Zheng, J.; Zhang, K.; Mo, S.; Lin, Z.; Pan, F. Mechanisms and properties of ion-transport in inorganic solid electrolytes. *Energy Storage Mater.* **2018**, *10*, 139–159. [[CrossRef](#)]
28. Reddy, M.V.; Julien, C.M.; Mauger, A.; Zaghbi, K. Sulfide and Oxide Inorganic Solid Electrolytes for All-Solid-State Li Batteries: A Review. *Nanomaterials* **2020**, *10*, 1606. [[CrossRef](#)]
29. Gao, Z.; Sun, H.; Fu, L.; Ye, F.; Zhang, Y.; Luo, W.; Huang, Y. Promises, challenges, and recent progress of inorganic solid-state electrolytes for all-solid-state lithium batteries. *Adv. Mater.* **2018**, *30*, 1705702. [[CrossRef](#)]
30. Chandra, A.; Bhatt, A.; Chandra, A. Ion Conduction in Superionic Glassy Electrolytes: An Overview. *J. Mater. Sci. Technol.* **2013**, *29*, 193–208. [[CrossRef](#)]
31. Funke, K.; Banhatti, R.D. Ionic motion in materials with disordered structures. *Solid State Ion.* **2006**, *177*, 1551–1557. [[CrossRef](#)]
32. Miura, A.; Rosero-Navarro, N.C.; Sakuda, A.; Tadanaga, K.; Phuc, N.H.H.; Matsuda, A.; Machida, N.; Hayashi, A.; Tatsumisago, M. Liquid-phase syntheses of sulfide electrolytes for all-solid-state lithium battery. *Nat. Rev. Chem.* **2019**, *3*, 189–198. [[CrossRef](#)]

33. Xu, R.; Xia, X.; Yao, Z.; Wang, X.; Gu, C.; Tu, J. Preparation of $\text{Li}_7\text{P}_3\text{S}_{11}$ glass-ceramic electrolyte by dissolution-evaporation method for all-solid-state lithium ion batteries. *Electrochim. Acta* **2016**, *219*, 235–240. [\[CrossRef\]](#)
34. Calpa, M.; Rosero-Navarro, N.C.; Miura, A.; Tadanaga, K. Instantaneous preparation of high lithium-ion conducting sulfide solid electrolyte $\text{Li}_7\text{P}_3\text{S}_{11}$ by a liquid phase process. *RSC Adv.* **2017**, *7*, 46499–46504. [\[CrossRef\]](#)
35. Choi, S.; Lee, S.; Park, J.; Nichols, W.T.; Shin, D. Facile synthesis of $\text{Li}_2\text{S-P}_2\text{S}_5$ glass-ceramics electrolyte with micron range particles for all-solid-state batteries via a low-temperature solution technique (LTST). *Appl. Surf. Sci.* **2018**, *444*, 10–14. [\[CrossRef\]](#)
36. Goodenough, J.B.; Hong, H.Y.P.; Kafalas, J.A. Fast Na^+ -ion transport in skeleton structures. *Mater. Res. Bull.* **1976**, *11*, 203–220. [\[CrossRef\]](#)
37. Thangadurai, V.; Weppner, W. Recent progress in solid oxide and lithium ion conducting electrolytes research. *Ionics* **2006**, *12*, 81–92. [\[CrossRef\]](#)
38. Mariappan, C.R.; Yada, C.; Rosciano, F.; Roling, B. Correlation between micro-structural properties and ionic conductivity of $\text{Li}_{1.5}\text{Al}_{0.5}\text{Ge}_{1.5}(\text{PO}_4)_3$ ceramics. *J. Power Sources* **2011**, *196*, 6456–6464. [\[CrossRef\]](#)
39. Mariappan, C.R.; Galven, C.; Crosnier-Lopez, M.P.; Le Berre, F.; Bohnke, O. Synthesis of nanostructured $\text{LiTi}_2(\text{PO}_4)_3$ powder by a pechini-type polymerizable complex method. *J. Solid State Chem.* **2006**, *179*, 450–456. [\[CrossRef\]](#)
40. Rossbach, A.; Tietz, F.; Grieshammer, S. Structural and transport properties of lithium-conducting NASICON materials. *J. Power Sources* **2018**, *391*, 1–9. [\[CrossRef\]](#)
41. Francisco, B.E.; Stoldt, C.R. Lithium-Ion Trapping from Local Structural Distortions in Sodium Super Ionic Conductor (NASICON) Electrolytes. *Chem. Mater.* **2014**, *26*, 4741–4749. [\[CrossRef\]](#)
42. Giarola, M.; Sanson, A.; Tietz, F.; Pristat, S.; Dashjav, E.; Rettenwander, D.; Redhammer, G.J.; Mariotto, G. Structure and vibrational dynamics of NASICON-type $\text{LiTi}_2(\text{PO}_4)_3$. *J. Phys. Chem. C* **2017**, *121*, 3697–3706. [\[CrossRef\]](#)
43. Narváez-Semanate, J.L.; Martins Rodrigues, A.C.; Muñoz-Meneses, R.A.; Muñoz-Hoyos, J.R.; Villamarín-Muñoz, J.A. Obtention and Characterization of Lithium Superionic Conductors Using the Glass-Ceramic Method. *Dyna* **2018**, *85*, 148–156. [\[CrossRef\]](#)
44. Pershina, S.V.; Antonov, B.D.; Farlenkov, A.S.; Vovkotrub, E.G. Glass-ceramics in $\text{Li}_{1+x}\text{Al}_x\text{Ge}_{2-x}(\text{PO}_4)_3$ system: The effect of Al_2O_3 addition on microstructure, structure and electrical properties. *J. Alloys Compd.* **2020**, *835*, 155281. [\[CrossRef\]](#)
45. Breuer, S.; Prutsch, D.; Ma, Q.; Epp, V.; Preishuber-Pflügl, F.; Tietzb, F.; Wilkening, M. Separating Bulk from Grain Boundary Li Ion Conductivity in the Sol-Gel Prepared Solid Electrolyte $\text{Li}_{1.5}\text{Al}_{0.5}\text{Ti}_{1.5}(\text{PO}_4)_3$. *J. Mater. Chem. A* **2015**, *3*, 21343–21350. [\[CrossRef\]](#)
46. Hartmann, P.; Leichtweiss, T.; Busche, M.R.; Schneider, M.; Reich, M.; Sann, J.; Adelhelm, P.; Janek, J. Degradation of NASICON-Type Materials in Contact with Lithium Metal: Formation of Mixed Conducting Interphases (MCI) on Solid Electrolytes. *J. Phys. Chem. C* **2013**, *117*, 21064–21074. [\[CrossRef\]](#)
47. Das, A.; Goswami, M.; Krishnan, M. Crystallization kinetics of $\text{Li}_2\text{O-Al}_2\text{O}_3\text{-GeO}_2\text{-P}_2\text{O}_5$ glass-ceramics system. *J. Therm. Anal. Calorim.* **2018**, *131*, 2421–2431. [\[CrossRef\]](#)
48. Feng, J.K.; Yan, B.G.; Liu, J.C.; Lai, M.O.; Li, L. All solid state lithium ion rechargeable batteries using NASICON structured electrolyte. *Mater. Technol.* **2013**, *28*, 276–279. [\[CrossRef\]](#)
49. He, K.; Zu, C.; Wang, Y.; Han, B.; Yin, X.; Zhao, H.; Liu, Y.; Chen, J. Stability of lithium ion conductor NASICON structure glass ceramic in acid and alkaline aqueous solution. *Solid State Ion.* **2014**, *254*, 78–81. [\[CrossRef\]](#)
50. Pershina, S.V.; Pankratov, A.A.; Vovkotrub, E.G.; Antonov, B.D. Promising high-conductivity $\text{Li}_{1.5}\text{Al}_{0.5}\text{Ge}_{1.5}(\text{PO}_4)_3$ solid electrolytes: The effect of crystallization temperature on the microstructure and transport properties. *Ionics* **2019**, *25*, 4713–4725. [\[CrossRef\]](#)
51. Illbeigi, M.; Fazlali, A.; Kazazi, M.; Mohammadi, A.M. Effect of simultaneous addition of aluminum and chromium on the lithium ionic conductivity of $\text{LiGe}_2(\text{PO}_4)_3$ NASICON-type glass-ceramics. *Solid State Ion.* **2016**, *289*, 180–187. [\[CrossRef\]](#)
52. Zhu, Y.; Zhang, Y.; Lu, L. Influence of crystallization temperature on ionic conductivity of lithium aluminum germanium phosphate glass-ceramic. *J. Power Sources* **2015**, *290*, 123–129. [\[CrossRef\]](#)
53. Nikodimos, Y.; Tsai, M.C.; Abrha, L.H.; Weldeyohannis, H.H.; Chiu, S.F.; Bezabh, H.K.; Shitaw, K.N.; Fenta, F.W.; Wu, S.H.; Su, W.N.; et al. Al-Sc Dual Doped $\text{LiGe}_2(\text{PO}_4)_3$ —A NASICON-Type Solid Electrolyte with Improved Ionic Conductivity. *J. Mater. Chem. A* **2020**, *8*, 11302–11313. [\[CrossRef\]](#)
54. Yi, E.; Wang, W.; Mohanty, S.; Kieffer, J.; Tamaki, R.; Laine, R.M. Materials that can replace liquid electrolytes in Li batteries: Superionic conductivities in $\text{Li}_{1.7}\text{Al}_{0.3}\text{Ti}_{1.7}\text{Si}_{0.4}\text{P}_{2.6}\text{O}_{12}$. Processing combustion synthesized nanopowders to free standing thin films. *J. Power Sources* **2014**, *269*, 577–588. [\[CrossRef\]](#)
55. Yan, B.; Kang, L.; Kotobuki, M.; Wang, F.; Huang, X.; Song, X.; Jiang, K. NASICON-structured solid-state electrolyte $\text{Li}_{1.5}\text{Al}_{0.5-x}\text{Ga}_x\text{Ge}_{1.5}(\text{PO}_4)_3$ prepared by microwave sintering. *Mater. Technol.* **2019**, *34*, 356–360. [\[CrossRef\]](#)
56. Wang, H.; Okubo, K.; Inada, M.; Hasegawa, G.; Enomoto, N.; Hayashi, K. Low temperature-densified NASICON-based ceramics promoted by $\text{Na}_2\text{O-Nb}_2\text{O}_5\text{-P}_2\text{O}_5$ glass additive and spark plasma sintering. *Solid State Ion.* **2018**, *322*, 54–60. [\[CrossRef\]](#)
57. Kobayashi, E.; Plashnitsa, L.S.; Doi, T.; Okada, S.; Yamaki, J.-I. Electrochemical properties of Li symmetric solid-state cell with NASICON-type solid electrolyte and electrodes. *Electrochem. Commun.* **2010**, *12*, 894–896. [\[CrossRef\]](#)
58. Thokchom, J.S.; Kumar, B. Microstructural Effects on the Superionic Conductivity of a Lithiated Glass-Ceramic. *Solid State Ion.* **2006**, *177*, 727–732. [\[CrossRef\]](#)
59. Zhong, Y.; Luo, J.; Shang, F.; Chen, G. Preparation, microstructure and ionic conductivity of $\text{Li}_{1.3}\text{Al}_{0.3}\text{Ti}_{1.7}(\text{PO}_4)_3/50\text{Li}_2\text{O-50P}_2\text{O}_5$ glass ceramic electrolytes. *J. Mater. Sci. Mater. Electron.* **2022**, *33*, 7869–7882. [\[CrossRef\]](#)

60. Leo, C.J.; Chowdari, B.V.R.; Rao, G.V.S.; Souquet, J.L. Lithium Conducting Glass Ceramic with Nasicon Structure. *Mater. Res. Bull.* **2002**, *37*, 1419–1430. [\[CrossRef\]](#)
61. Santagneli, S.H.; Baldacim, H.V.A.; Ribeiro, S.J.L.; Kundu, S.; Rodrigues, A.C.M.; Doerenkamp, C.; Eckert, H. Preparation, Structural Characterization, and Electrical Conductivity of Highly Ion-Conducting Glasses and Glass Ceramics in the System $\text{Li}_{1+x}\text{Al}_x\text{Sn}_y\text{Ge}_{2-(x+y)}(\text{PO}_4)_3$. *J. Phys. Chem. C* **2016**, *120*, 14556–14567. [\[CrossRef\]](#)
62. Xu, X.; Wen, Z.; Wu, X.; Yang, X.; Gu, Z. Lithium Ion Conducting Glass-Ceramics of $\text{Li}_{1.5}\text{Al}_{0.5}\text{Ge}_{1.5}(\text{PO}_4)_3-x\text{Li}_2\text{O}$ ($x = 0.0-0.20$) with Good Electrical and Electrochemical Properties. *J. Am. Ceram. Soc.* **2007**, *90*, 2802–2806. [\[CrossRef\]](#)
63. Pershina, S.V.; Vovkotrub, E.G.; Antonov, B.D. Effects of B_2O_3 on crystallization kinetics, microstructure and properties of $\text{Li}_{1.5}\text{Al}_{0.5}\text{Ge}_{1.5}(\text{PO}_4)_3$ -based glass-ceramics. *Solid State Ion.* **2022**, *383*, 115990. [\[CrossRef\]](#)
64. Nuernberg, R.B.; Rodrigues, A.C.M. A New NASICON Lithium Ion- Conducting Glass-Ceramic of the $\text{Li}_{1+x}\text{Cr}_x(\text{Ge}_y\text{Ti}_{1-y})_{2-x}(\text{PO}_4)_3$ System. *Solid State Ion.* **2017**, *301*, 1–9. [\[CrossRef\]](#)
65. Nuernberg, R.B.; Pradel, A.; Rodrigues, A.C.M. A systematic study of glass stability, crystal structure and electrical properties of lithium ion-conducting glass-ceramics of the $\text{Li}_{1+x}\text{Cr}_x(\text{Ge}_y\text{Ti}_{1-y})_{2-x}(\text{PO}_4)_3$ system. *J. Power Sources* **2017**, *371*, 167–177. [\[CrossRef\]](#)
66. Nagao, K.; Hayashi, A.; Tatsumisago, M. Mechanochemical synthesis and crystallization of $\text{Li}_3\text{BO}_3\text{-Li}_2\text{CO}_3$ glass electrolytes. *J. Ceram. Soc. Jpn.* **2016**, *124*, 915–919. [\[CrossRef\]](#)
67. Tatsumisago, M.; Takano, R.; Nose, M.; Nagao, K.; Kato, A.; Sakuda, A.; Tadanaga, K.; Hayashi, A. Electrical and mechanical properties of glass and glass-ceramic electrolytes in the system $\text{Li}_3\text{BO}_3\text{-Li}_2\text{SO}_4$. *J. Ceram. Soc. Jpn.* **2017**, *125*, 433–437. [\[CrossRef\]](#)
68. Yoneda, Y.; Shigeno, M.; Kimura, T.; Nagao, K.; Hotehama, C.; Sakuda, A.; Tatsumisago, M.; Hayashi, A. Preparation and characterization of hexagonal Li_4GeO_4 -based glass-ceramic electrolytes. *Solid State Ion.* **2021**, *363*, 115605. [\[CrossRef\]](#)
69. Tatsumisago, M.; Takano, R.; Tadanaga, K.; Hayashi, A. Preparation of $\text{Li}_3\text{BO}_3\text{-Li}_2\text{SO}_4$ glass-ceramic electrolytes for all-oxide lithium batteries. *J. Power Sources* **2014**, *270*, 603–607. [\[CrossRef\]](#)
70. Yoneda, Y.; Hotehama, C.; Sakuda, A.; Tatsumisago, M.; Hayashi, A. Glassy oxide electrolytes in the system $\text{Li}_4\text{SiO}_4\text{-Li}_2\text{SO}_4$ with excellent formability. *J. Ceram. Soc. Jpn.* **2021**, *129*, 458–463. [\[CrossRef\]](#)
71. Widanarto, W.; Ramdhan, A.M.; Ghoshal, S.K.; Effendi, M.; Cahyanto, W.T. Improved ionic conductivity of lithium-zinc-tellurite glass-ceramic electrolytes. *Results Phys.* **2017**, *7*, 2277–2280. [\[CrossRef\]](#)
72. Tezuka, N.; Okawa, Y.; Kajihara, K.; Kanamura, K. Synthesis and characterization of lithium-ion-conductive glass-ceramics of lithium chloroborate $\text{Li}_{4+x}\text{B}_7\text{O}_{12+x/2}\text{Cl}$ ($x = 0-1$). *J. Ceram. Soc. Jpn.* **2017**, *125*, 348–352. [\[CrossRef\]](#)
73. Nagao, K.; Nose, M.; Kato, A.; Sakuda, A.; Hayashi, A.; Tatsumisago, M. Preparation and characterization of glass solid electrolytes in the pseudoternary system $\text{Li}_3\text{BO}_3\text{-Li}_2\text{SO}_4\text{-Li}_2\text{CO}_3$. *Solid State Ion.* **2017**, *308*, 68–76. [\[CrossRef\]](#)
74. Okumura, T.; Takeuchi, T.; Kobayashi, H. Enhancement of lithium-ion conductivity for $\text{Li}_{2.2}\text{C}_{0.8}\text{B}_{0.2}\text{O}_3$ by spark plasma sintering. *J. Ceram. Soc. Jpn.* **2017**, *125*, 276–280. [\[CrossRef\]](#)
75. Shin, R.-H.; Son, S.I.; Han, Y.S.; Kim, Y.D.; Kim, H.-T.; Ryu, S.-S.; Pan, W. Sintering behavior of garnet-type $\text{Li}_7\text{La}_3\text{Zr}_2\text{O}_{12}\text{-Li}_3\text{BO}_3$ composite solid electrolytes for all-solid-state lithium batteries. *Solid State Ion.* **2017**, *301*, 10–14. [\[CrossRef\]](#)
76. Tatsumisago, M.; Hayashi, A. Superionic glasses and glass-ceramics in the $\text{Li}_2\text{S-P}_2\text{S}_5$ system for all-solid-state lithium secondary batteries. *Solid State Ion.* **2012**, *225*, 342–345. [\[CrossRef\]](#)
77. Mi, C.; Hall, S.R. Preparation and degradation of high air stability sulfide solid electrolyte $75\text{Li}_2\text{S-}25\text{P}_2\text{S}_5$ glass-ceramic. *Solid State Ion.* **2023**, *389*, 116106. [\[CrossRef\]](#)
78. Zhang, Y.; Chen, R.; Liu, T.; Shen, Y.; Lin, Y.; Nan, C.W. High Capacity, Superior Cyclic Performances in All-Solid-State Lithium-Ion Batteries Based on $78\text{Li}_2\text{S-}22\text{P}_2\text{S}_5$ Glass-Ceramic Electrolytes Prepared via Simple Heat Treatment. *ACS Appl. Mater. Interfaces* **2017**, *9*, 28542–28548. [\[CrossRef\]](#)
79. Yamane, H.; Shibata, M.; Shimane, Y.; Junke, T.; Seino, Y.; Adams, S.; Minami, K.; Hayashi, A.; Tatsumisago, M. Crystal Structure of a Superionic Conductor, $\text{Li}_7\text{P}_3\text{S}_{11}$. *Solid State Ion.* **2007**, *178*, 1163–1167. [\[CrossRef\]](#)
80. Wang, Y.; Richards, W.D.; Ong, S.P.; Miara, L.J.; Kim, J.C.; Mo, Y.; Ceder, G. Design Principles for Solid-State Lithium Superionic Conductors. *Nat. Mater.* **2015**, *14*, 1026–1031. [\[CrossRef\]](#)
81. Ohtomo, T.; Hayashi, A.; Tatsumisago, M.; Tsuchida, Y.; Hama, S.; Kawamoto, K. All-solid-state lithium secondary batteries using the $75\text{Li}_2\text{S-}25\text{P}_2\text{S}_5$ glass and the $70\text{Li}_2\text{S-}30\text{P}_2\text{S}_5$ glass-ceramic as solid electrolytes. *J. Power Sources* **2013**, *233*, 231–235. [\[CrossRef\]](#)
82. Homma, K.; Yonemura, M.; Kobayashi, T.; Nagao, M.; Hirayama, M.; Kanno, R. Crystal structure and phase transitions of the lithium ionic conductor Li_3PS_4 . *Solid State Ion.* **2011**, *182*, 53–58. [\[CrossRef\]](#)
83. Chen, S.; Xie, D.; Liu, G.; Mwizerwa, J.P.; Zhang, Q.; Zhao, Y.; Xu, X.; Yao, X. Sulfide Solid Electrolytes for All-Solid-State Lithium Batteries: Structure, Conductivity, Stability and Application. *Energy Storage Mater.* **2018**, *14*, 58–74. [\[CrossRef\]](#)
84. Kim, J.; Yoon, Y.; Lee, J.; Shin, D. Formation of the high lithium ion conducting phase from mechanically milled amorphous $\text{Li}_2\text{S-P}_2\text{S}_5$ system. *J. Power Sources* **2011**, *196*, 6920–6923. [\[CrossRef\]](#)
85. Lu, S.; Kosaka, F.; Shiotani, S.; Tsukasaki, H.; Mori, S.; Otomo, J. Optimization of lithium ion conductivity of $\text{Li}_2\text{S-P}_2\text{S}_5$ glass ceramics by microstructural control of crystallization kinetics. *Solid State Ion.* **2021**, *362*, 115583. [\[CrossRef\]](#)
86. Yu, C.; Ganapathy, S.; van Eck, E.R.; van Eijck, L.; de Klerk, N.; Kelder, E.M.; Wagemaker, M. Investigation of Li-ion transport in $\text{Li}_7\text{P}_3\text{S}_{11}$ and solid-state lithium batteries. *J. Energy Chem.* **2019**, *38*, 1–7. [\[CrossRef\]](#)
87. Wang, R.; Wu, Z.; Yu, C.; Wei, C.; Peng, L.; Wang, L.; Cheng, S.; Xie, J. Low temperature ensures FeS_2 cathode superior cycling stability in $\text{Li}_7\text{P}_3\text{S}_{11}$ -based all-solid-state lithium batteries. *Front. Energy Res.* **2023**, *10*, 1108789. [\[CrossRef\]](#)

88. Trevey, J.E.; Jung, Y.S.; Lee, S. High lithium ion conducting $\text{Li}_2\text{S-GeS}_2\text{-P}_2\text{S}_5$ glass-ceramic solid electrolyte with sulfur additive for all solid-state lithium secondary batteries. *Electrochim. Acta* **2011**, *56*, 4243–4247. [\[CrossRef\]](#)
89. Seino, Y.; Ota, T.; Takada, K.; Hayashi, A.; Tatsumisago, M. A sulphide lithium super ion conductor is superior to liquid ion conductors for use in rechargeable batteries. *Energy Environ. Sci.* **2014**, *7*, 627–631. [\[CrossRef\]](#)
90. Preefer, M.B.; Grebenkemper, J.H.; Schroeder, F.; Bocarsly, J.D.; Pilar, K.; Cooley, J.A.; Zhang, W.; Hu, J.; Misra, S.; Seeler, F.; et al. Rapid and Tunable Assisted-Microwave Preparation of Glass and Glass-Ceramic Thiophosphate “ $\text{Li}_7\text{P}_3\text{S}_{11}$ ” Li-Ion Conductors. *ACS Appl. Mater. Interfaces* **2019**, *11*, 42280–42287. [\[CrossRef\]](#)
91. Muramatsu, H.; Hayashi, A.; Ohtomo, T.; Hama, S.; Tatsumisago, M. Structural change of $\text{Li}_2\text{S-P}_2\text{S}_5$ sulfide solid electrolytes in the atmosphere. *Solid State Ion.* **2011**, *182*, 116–119. [\[CrossRef\]](#)
92. Trevey, J.E.; Jung, Y.S.; Lee, S. Preparation of $\text{Li}_2\text{S-GeSe}_2\text{-P}_2\text{S}_5$ electrolytes by a single step ball milling for all-solid-state lithium secondary batteries. *J. Power Sources* **2010**, *195*, 4984–4989. [\[CrossRef\]](#)
93. Kim, J.; Yoon, Y.; Eom, M.; Shin, D. Characterization of amorphous and crystalline $\text{Li}_2\text{S-P}_2\text{S}_5\text{-P}_2\text{Se}_5$ solid electrolytes for all-solid-state lithium ion batteries. *Solid State Ion.* **2012**, *225*, 626–630. [\[CrossRef\]](#)
94. Lu, P.; Ding, F.; Xu, Z.; Liu, J.; Liu, X.; Xu, Q. Study on $(100 - x)(70\text{Li}_2\text{S-30P}_2\text{S}_5)\text{-xLi}_2\text{ZrO}_3$ glass-ceramic electrolyte for all-solid-state lithium-ion batteries. *J. Power Sources* **2017**, *356*, 163–171. [\[CrossRef\]](#)
95. Choi, S.; Eom, M.; Park, C.; Son, S.; Lee, G.; Shin, D. Effect of Li_2SO_4 on the properties of $\text{Li}_2\text{S-P}_2\text{S}_5$ glass-ceramic solid electrolytes. *Ceram. Int.* **2016**, *42*, 6738–6742. [\[CrossRef\]](#)
96. Trevey, J.E.; Gilsdorf, J.R.; Miller, S.W.; Lee, S. $\text{Li}_2\text{S-Li}_2\text{O-P}_2\text{S}_5$ solid electrolyte for all-solid-state lithium batteries. *Solid State Ion.* **2012**, *214*, 25–30. [\[CrossRef\]](#)
97. Liu, G.; Xie, D.; Wang, X.; Yao, X.; Chen, S.; Xiao, R.; Li, H.; Xu, X. High air-stability and superior lithium ion conduction of $\text{Li}_{3+3x}\text{P}_{1-x}\text{Zn}_x\text{S}_{4-x}\text{O}_x$ by aliovalent substitution of ZnO for all-solid-state lithium batteries. *Energy Storage Mater.* **2019**, *17*, 266–274. [\[CrossRef\]](#)
98. Ahmad, N.; Sun, S.; Yu, P.; Yang, W. Design Unique Air-Stable and Li-Metal Compatible Sulfide Electrolyte via Exploration of Anion Functional Units for All-Solid-State Lithium-Metal Batteries. *Adv. Funct. Mater.* **2022**, *32*, 2201528. [\[CrossRef\]](#)
99. Jiang, Z.; Liang, T.; Liu, Y.; Zhang, S.; Li, Z.; Wang, D.; Wang, X.; Xia, X.; Gu, C.; Tu, J. Improved Ionic Conductivity and Li Dendrite Suppression Capability toward $\text{Li}_7\text{P}_3\text{S}_{11}$ -Based Solid Electrolytes Triggered by Nb and O Cosubstitution. *ACS Appl. Mater. Interfaces* **2020**, *12*, 54662–54670. [\[CrossRef\]](#)
100. Huang, B.; Yao, X.; Huang, Z.; Guan, Y.; Jin, Y.; Xu, X. Li_3PO_4 -doped $\text{Li}_7\text{P}_3\text{S}_{11}$ glass-ceramic electrolytes with enhanced lithium ion conductivities and application in all-solid-state batteries. *J. Power Sources* **2019**, *284*, 206–211. [\[CrossRef\]](#)
101. Tsukasaki, H.; Morimoto, H.; Mori, S. Thermal behavior and microstructure of the $\text{Li}_3\text{PS}_4\text{-ZnO}$ composite electrolyte. *J. Power Sources* **2019**, *436*, 226865. [\[CrossRef\]](#)
102. Minami, K.; Hayashi, A.; Tatsumisago, M. Preparation and Characterization of Lithium Ion Conducting $\text{Li}_2\text{S-P}_2\text{S}_5\text{-GeS}_2$ Glasses and Glass -Ceramics. *J. Non-Cryst. Solids* **2010**, *356*, 2666–2669. [\[CrossRef\]](#)
103. Hayashi, A.; Minami, K.; Ujiie, S.; Tatsumisago, M. Preparation and Ionic Conductivity of $\text{Li}_7\text{P}_3\text{S}_{11-z}$ Glass-Ceramic Electrolytes. *J. Non-Cryst. Solids* **2010**, *356*, 2670–2673. [\[CrossRef\]](#)
104. Park, C.; Lee, S.; Kim, M.; Min, S.; Kim, G.; Park, S.; Shin, D. Li metal stability enhancement of Sn-doped $\text{Li}_2\text{S-P}_2\text{S}_5$ glass-ceramics electrolyte. *Electrochim. Acta* **2021**, *390*, 138808. [\[CrossRef\]](#)
105. Park, M.; Jung, H.-G.; Jung, W.D.; Cho, S.Y.; Yun, B.-N.; Lee, Y.S.; Choi, S.; Ahn, J.; Lim, J.; Sung, J.Y.; et al. Chemically Evolved Composite Lithium-Ion Conductors with Lithium Thiophosphates and Nickel Sulfides. *ACS Energy Lett.* **2017**, *2*, 1740–1745. [\[CrossRef\]](#)
106. Dong, P.; Jiao, Q.; Zhang, Z.; Jiang, M.; Lin, C.; Zhang, X.; Ma, H.; Ma, B.; Dai, S.; Xu, T. Controllable $\text{Li}_3\text{PS}_4\text{-Li}_4\text{SnS}_4$ solid electrolytes with affordable conductor and high conductivity for solid-state battery. *J. Am. Ceram. Soc.* **2022**, *105*, 3252–3260. [\[CrossRef\]](#)
107. Zhou, L.; Tufail, M.K.; Yang, L.; Ahmad, N.; Chen, R.; Yang, W. Cathode-doped sulfide electrolyte strategy for boosting all-solid-state lithium batteries. *Chem. Eng. J.* **2020**, *391*, 123529. [\[CrossRef\]](#)
108. Otoyama, M.; Kuratani, K.; Kobayashi, H. A systematic study on structure, ionic conductivity, and air-stability of $x\text{Li}_4\text{SnS}_4\cdot(1-x)\text{Li}_3\text{PS}_4$ solid electrolytes. *Ceram. Int.* **2021**, *47*, 28377–28383. [\[CrossRef\]](#)
109. Han, F.; Yue, J.; Zhu, X.; Wang, C. Suppressing Li Dendrite Formation in $\text{Li}_2\text{S-P}_2\text{S}_5$ Solid Electrolyte by LiI Incorporation. *Adv. Energy Mater.* **2018**, *8*, 1703644. [\[CrossRef\]](#)
110. Bui, A.D.; Choi, S.H.; Choi, H.; Lee, Y.J.; Doh, C.H.; Park, J.W.; Kim, B.G.; Lee, W.J.; Lee, S.M.; Ha, Y.C. Origin of the Outstanding Performance of Dual Halide Doped $\text{Li}_7\text{P}_2\text{S}_8\text{X}$ ($\text{X} = \text{I}, \text{Br}$) Solid Electrolytes for All-Solid-State Lithium Batteries. *ACS Appl. Energy Mater.* **2021**, *4*, 1–8. [\[CrossRef\]](#)
111. El Kharbachi, A.; Hu, Y.; Yoshida, K.; Vajeeston, P.; Kim, S.; Sørby, M.H.; Orimo, S.-I.; Fjellvåg, H.; Hauback, B.C. Lithium ionic conduction in composites of $\text{Li}(\text{BH}_4)_{0.75}\text{I}_{0.25}$ and amorphous $0.75\text{Li}_2\text{S-0.25P}_2\text{S}_5$ for battery applications. *Electrochim. Acta* **2018**, *278*, 332–339. [\[CrossRef\]](#)
112. Ujiie, S.; Inagaki, T.; Hayashi, A.; Tatsumisago, M. Conductivity of $70\text{Li}_2\text{S-30P}_2\text{S}_5$ glasses and glass-ceramics added with lithium halides. *Solid State Ion.* **2014**, *263*, 57–61. [\[CrossRef\]](#)
113. Zhao, B.; Wu, J.; Wang, Z.; Ma, W.; Shi, Y.; Jiang, Y.; Jiang, J.; Liu, X.; Xu, Y.; Zhang, J. Incorporation of lithium halogen in $\text{Li}_7\text{P}_3\text{S}_{11}$ glass-ceramic and the interface improvement mechanism. *Electrochim. Acta* **2021**, *390*, 138849. [\[CrossRef\]](#)

114. Zhang, N.; Ding, F.; Yu, S.; Zhu, K.; Li, H.; Zhang, W.; Liu, X.; Xu, Q. Novel Research Approach Combined with Dielectric Spectrum Testing for Dual-Doped $\text{Li}_7\text{P}_3\text{S}_{11}$ Glass-Ceramic Electrolytes. *ACS Appl. Mater. Interfaces* **2019**, *11*, 27897–27905. [\[CrossRef\]](#) [\[PubMed\]](#)
115. Wang, G.; Liang, B.; Lin, C.; Gao, C.; Shen, X.; Liu, Y.; Jiao, Q. Design of cation doped $\text{Li}_7\text{P}_2\text{S}_8\text{Br}_{(1-x)}\text{I}_x$ sulfide electrolyte with improved conductivity and stable interfacial properties for all-solid-state lithium batteries. *Appl. Mater. Today* **2022**, *29*, 101692. [\[CrossRef\]](#)
116. Jung, W.D.; Yun, B.N.; Jung, H.G.; Choi, S.; Son, J.W.; Lee, J.H.; Lee, J.H.; Kim, H. Configuring PS_x tetrahedral clusters in Li-excess $\text{Li}_7\text{P}_3\text{S}_{11}$ solid electrolyte. *APL Mater.* **2018**, *6*, 047902. [\[CrossRef\]](#)
117. Wei, J.; Kim, H.; Lee, D.-C.; Hu, R.; Wu, F.; Zhao, H.; Alamgir, F.M.; Yushin, G. Influence of annealing on ionic transfer and storage stability of Li_2S - P_2S_5 solid electrolyte. *J. Power Sources* **2015**, *294*, 494–500. [\[CrossRef\]](#)
118. Raj, V.; Aetukuri, N.P.B.; Nanda, J. Solid state lithium metal batteries-Issues and challenges at the lithium-solid electrolyte interface. *Curr. Opin. Solid State Mater. Sci.* **2022**, *26*, 100999. [\[CrossRef\]](#)
119. Sun, C.; Liu, J.; GongGong, Y. Recent advances in all-solid-state rechargeable lithium batteries. *Nano Energy* **2017**, *33*, 363–386. [\[CrossRef\]](#)
120. Agostini, M.; Aihara, Y.; Yamada, T.; Scrosati, B.; Hassoun, J. A lithium-sulfur battery using a solid, glass-type P_2S_5 - Li_2S electrolyte. *Solid State Ion.* **2013**, *244*, 48–51. [\[CrossRef\]](#)
121. Fu, K.; Gong, Y.; Xu, S.; Zhu, Y.; Li, Y.; Dai, J.; Wang, C.; Liu, B.; Pastel, G.; Xie, H.; et al. Stabilizing the garnet solid-electrolyte/polysulfide interface in Li-S batteries. *Chem. Mater.* **2017**, *29*, 8037–8041. [\[CrossRef\]](#)
122. Umeshbabu, E.; Zheng, B.; Yang, Y. Recent Progress in All-Solid-State Lithium-Sulfur Batteries Using High Li-Ion Conductive Solid Electrolytes. *Electrochem. Energy Rev.* **2019**, *2*, 199–230. [\[CrossRef\]](#)
123. Tufail, M.K.; Ahmad, N.; Zhou, L.; Faheem, M.; Yang, L.; Chen, R.; Yang, W. Insight on air-induced degradation mechanism of $\text{Li}_7\text{P}_3\text{S}_{11}$ to design a chemical-stable solid electrolyte with high Li_2S utilization in all-solid-state Li/S batteries. *Chem. Eng. J.* **2021**, *425*, 130535. [\[CrossRef\]](#)
124. Sun, Y.-Y.; Zhang, Q.; Yan, L.; Wang, T.-B.; Hou, P.-Y. A review of interfaces within solid-state electrolytes: Fundamentals, issues and advancements. *Chem. Eng. J.* **2022**, *437*, 135179. [\[CrossRef\]](#)
125. Yu, S.; Siegel, D.J. Grain boundary contributions to Li-ion transport in the solid electrolyte $\text{Li}_7\text{La}_3\text{Zr}_2\text{O}_{12}$ (LLZO). *Chem. Mater.* **2017**, *29*, 9639–9647. [\[CrossRef\]](#)
126. Shin, B.R.; Nam, Y.J.; Oh, D.Y.; Kim, D.H.; Kim, J.W.; Jung, Y.S. Comparative Study of TiS_2 /Li-In All-Solid-State Lithium Batteries Using Glass-Ceramic Li_3PS_4 and $\text{Li}_{10}\text{GeP}_2\text{S}_{12}$ Solid Electrolytes. *Electrochim. Acta* **2014**, *146*, 395–402. [\[CrossRef\]](#)
127. Wang, C.; Yang, Y.; Liu, X.; Zhong, H.; Xu, H.; Xu, Z.; Shao, H.; Ding, F. Suppression of Lithium Dendrite Formation by Using LAGP-PEO (LiTFSI) Composite Solid Electrolyte and Lithium Metal Anode Modified by PEO (LiTFSI) in All-Solid-State Lithium Batteries. *ACS Appl. Mater. Interfaces* **2017**, *9*, 13694–13702. [\[CrossRef\]](#)
128. Zhou, X.; Zhang, Y.; Shen, M.; Fang, Z.; Kong, T.; Feng, W.; Xie, Y.; Wang, F.; Hu, B.; Wang, Y. A Highly Stable Li-Organic All-Solid-State Battery Based on Sulfide Electrolytes. *Adv. Energy Mater.* **2022**, *12*, 2103932. [\[CrossRef\]](#)
129. Manthiram, A.; Yu, X.; Wang, S. Lithium battery chemistries enabled by solid-state electrolytes. *Nat. Rev. Mater.* **2017**, *2*, 16103. [\[CrossRef\]](#)
130. Sumita, M.; Tanaka, Y.; Ikeda, M.; Ohno, T. Charged and Discharged States of Cathode/Sulfide Electrolyte Interfaces in All-Solid-State Lithium-Ion Batteries. *J. Phys. Chem. C* **2016**, *120*, 13332–13339. [\[CrossRef\]](#)
131. Kato, A.; Hayashi, A.; Tatsumisago, M. Enhancing utilization of lithium metal electrodes in all-solid-state batteries by interface modification with gold thin films. *J. Power Sources* **2016**, *309*, 27–32. [\[CrossRef\]](#)
132. Liang, J.-Y.; Zeng, X.-X.; Zhang, X.-D.; Wang, P.-F.; Ma, J.-Y.; Yin, Y.-X.; Wu, X.-W.; Guo, Y.-G.; Wan, L.-J. Mitigating Interfacial Potential Drop of Cathode-Solid Electrolyte via Ionic Conductor Layer To Enhance Interface Dynamics for Solid Batteries. *J. Am. Chem. Soc.* **2018**, *140*, 6767–6770. [\[CrossRef\]](#) [\[PubMed\]](#)
133. Jadhav, H.S.; Cho, M.-S.; Kalubarme, R.S.; Lee, J.-S.; Jung, K.-N.; Shin, K.-H.; Park, C.-J. Influence of B_2O_3 addition on the ionic conductivity of $\text{Li}_{1.5}\text{Al}_{0.5}\text{Ge}_{1.5}(\text{PO}_4)_3$ glass ceramics. *J. Power Sources* **2013**, *241*, 502–508. [\[CrossRef\]](#)
134. Saffirio, S.; Falco, M.; Appetecchi, G.B.; Smeacetto, F.; Gerbaldi, C. $\text{Li}_{1.4}\text{Al}_{0.4}\text{Ge}_{0.4}\text{Ti}_{1.4}(\text{PO}_4)_3$ promising NASICON-structured glass-ceramic electrolyte for all-solid-state Li-based batteries: Unravelling the effect of diboron trioxide. *J. Eur. Ceram. Soc.* **2022**, *42*, 1023–1032. [\[CrossRef\]](#)
135. Yamamoto, K.; Yoshida, R.; Sato, T.; Matsumoto, H.; Kurobe, H.; Hamanaka, T.; Kato, T.; Iriyama, Y.; Hirayama, T. Nano-scale simultaneous observation of Li-concentration profile and Ti-, O electronic structure changes in an all-solid-state Li-ion battery by spatially-resolved electron energy-loss spectroscopy. *J. Power Sources* **2014**, *266*, 414–421. [\[CrossRef\]](#)
136. Liu, Y.; Li, C.; Li, B.; Song, H.; Cheng, Z.; Chen, M.; He, P.; Zhou, H. Germanium Thin Film Protected Lithium Aluminum Germanium Phosphate for Solid-State Li Batteries. *Adv. Energy Mater.* **2018**, *8*, 1702374. [\[CrossRef\]](#)
137. Hu, F.; Li, Y.; Wei, Y.; Yang, J.; Hu, P.; Rao, Z.; Chen, X.; Yuan, L.; Li, Z. Construct an Ultrathin Bismuth Buffer for Stable Solid-State Lithium Metal Batteries. *ACS Appl. Mater. Interfaces* **2020**, *12*, 12793–12800. [\[CrossRef\]](#)
138. Yamamoto, Y.; Iriyama, Y.; Muto, S. STEM-EELS analysis of the interface structures of composite ASSLIB electrodes fabricated via aerosol deposition. *J. Am. Ceram. Soc.* **2020**, *103*, 1454–1462. [\[CrossRef\]](#)

139. Shubha, N.; Prasanth, R.; Hng, H.H.; Srinivasan, M. Study on effect of poly (ethylene oxide) addition and in-situ porosity generation on poly (vinylidene fluoride)-glass ceramic composite membranes for lithium polymer batteries. *J. Power Sources* **2014**, *267*, 48–57. [[CrossRef](#)]
140. Wu, Z.; Xie, Z.; Yoshida, A.; An, X.; Wang, Z.; Hao, X.; Abudula, A.; Guan, G. Novel SeS₂ doped Li₂S-P₂S₅ solid electrolyte with high ionic conductivity for all-solid-state lithium sulfur batteries. *Chem. Eng. J.* **2020**, *380*, 122419.
141. Feng, X.; Chien, P.-H.; Patel, S.; Zheng, J.; Immediato-Scuotto, M.; Xin, Y.; Hung, I.; Gan, Z.; Hu, Y.-Y. Synthesis and characterizations of highly conductive and stable electrolyte Li₁₀P₃S₁₂I. *Energy Storage Mater.* **2019**, *22*, 397–401. [[CrossRef](#)]
142. Xu, R.; Han, F.; Ji, X.; Fan, X.; Tu, J.; Wang, C. Interface engineering of sulfide electrolytes for all-solid-state lithium batteries. *Nano Energy* **2018**, *53*, 958–966. [[CrossRef](#)]

Disclaimer/Publisher's Note: The statements, opinions and data contained in all publications are solely those of the individual author(s) and contributor(s) and not of MDPI and/or the editor(s). MDPI and/or the editor(s) disclaim responsibility for any injury to people or property resulting from any ideas, methods, instructions or products referred to in the content.